2024-02-08

Antigen-presenting autoreactive B cells activate regulatory T cells and suppress autoimmune arthritis in mice

Aoun, Mike; Coelho, Ana; Krämer, Alexander; Saxena, Amit; Sabatier, Pierre; Beusch, Christian Michel; Lönnblom, Erik; Geng, Manman; Do, Nhu-Nguyen; Xu, Zhongwei; Zhang, Jingdian; He, Yibo; Romero Castillo, Laura; Abolhassani, Hassan; Xu, Bingze; Viljanen, Johan; Rorbach, Joanna; Fernandez Lahore, Gonzalo; Gjertsson, Inger; Kastbom, Alf; Sjöwall, Christopher; Kihlberg, Jan; Zubarev, Roman A; Burkhardt, Harald; Holmdahl, Rikard

J Exp Med . 2023 Nov 6;220(11):e20230101. doi: 10.1084/jem.20230101. Epub 2023 Sep 11.
New York, NY : Rockefeller University Press
http://doi.org/10.1084/jem.20230101
http://hdl.handle.net/10616/48998

JEM Journal of Experimental Medicine

ARTICLE

Antigen-presenting autoreactive B cells activate regulatory T cells and suppress autoimmune arthritis in mice

Mike Aoun[1], Ana Coelho[1*], Alexander Krämer[1*], Amit Saxena[1*], Pierre Sabatier[2], Christian Michel Beusch[2], Erik Lönnblom[1], Manman Geng[3], Nhu-Nguyen Do[1,4], Zhongwei Xu[1], Jingdian Zhang[5,6], Yibo He[1], Laura Romero Castillo[1], Hassan Abolhassani[7], Bingze Xu[1], Johan Viljanen[8], Joanna Rorbach[5,6], Gonzalo Fernandez Lahore[1], Inger Gjertsson[9], Alf Kastbom[10], Christopher Sjöwall[10], Jan Kihlberg[8], Roman A. Zubarev[2,11], Harald Burkhardt[4,12], and Rikard Holmdahl[1,3]

B cells undergo several rounds of selection to eliminate potentially pathogenic autoreactive clones, but in contrast to T cells, evidence of positive selection of autoreactive B cells remains moot. Using unique tetramers, we traced natural autoreactive B cells (C1-B) specific for a defined triple-helical epitope on collagen type-II (COL2), constituting a sizeable fraction of the physiological B cell repertoire in mice, rats, and humans. Adoptive transfer of C1-B suppressed arthritis independently of IL10, separating them from IL10-secreting regulatory B cells. Single-cell sequencing revealed an antigen processing and presentation signature, including induced expression of CD72 and CCR7 as surface markers. C1-B presented COL2 to T cells and induced the expansion of regulatory T cells in a contact-dependent manner. CD72 blockade impeded this effect suggesting a new downstream suppressor mechanism that regulates antigen-specific T cell tolerization. Thus, our results indicate that autoreactive antigen-specific naïve B cells tolerize infiltrating T cells against self-antigens to impede the development of tissue-specific autoimmune inflammation.

Introduction

It is well established that autoreactive B cells can be functionally impaired or deleted in the bone marrow (BM) after exposure to self-antigens (Goodnow et al., 1988; Nemazee and Bürki, 1989). However, recent studies show that many autoreactive B cells survive BM development, and their responsiveness could be tuned by endogenous antigens (Zikherman et al., 2012). Yet, conclusive evidence for the selection of autoreactive B cells (conventional B2 cells) under physiological conditions and an explanation for this phenomenon remain elusive.

Defect in tolerance mechanisms may cause autoimmune disease, like rheumatoid arthritis (RA), where the frequency of BM-derived polyreactive B cells are elevated and may cause the overproduction of disease-associated autoantibodies (Samuels et al., 2005). It is possible that the arrest of the autoreactive B cell in the BM contributes to protection against autoimmune disease, but the physiologic presence of autoreactive B cells could also imply regulatory functions. In mice, immunization with type II collagen (COL2) induces a drastic B cell response leading to polyarthritis, known as collagen-induced arthritis (CIA), which is the prime animal model for RA (Holmdahl et al., 1990). Interestingly, the presence of autoreactive B cells suggests that these B cells are not negatively selected. The early response is dominated by germline-encoded IgG antibodies (Mo et al., 1993; Mo et al., 1994), hypothesizing the presence of COL2-specific B cells within the B cell repertoire under physiologic conditions. In fact, COL2 predominates in cartilage (Gottardi

[1]Division of Medical Inflammation Research, Department of Medical Biochemistry and Biophysics, Karolinska Institute, Solna, Sweden; [2]Division of Physiological Chemistry I, Department of Medical Biochemistry and Biophysics, Karolinska Institute, Solna, Sweden; [3]Precision Medicine Institute, The Second Affiliated Hospital of Xi'an Jiaotong University, Xi'an, China; [4]Fraunhofer Institute for Translational Medicine and Pharmacology, and Fraunhofer Cluster of Excellence for Immune-Mediated Diseases, Frankfurt am Main, Germany; [5]Max Planck Institute Biology of Ageing—Karolinska Institute Laboratory, Karolinska Institute, Solna, Sweden; [6]Division of Molecular Metabolism, Department of Medical Biochemistry and Biophysics, Karolinska Institute, Solna, Sweden; [7]Division of Clinical Immunology, Department of Biosciences and Nutrition, Karolinska Institutet, Karolinska University Hospital, Neo Building, Solna, Sweden; [8]Department of Chemistry, Biomedical Center, Uppsala University, Uppsala, Sweden; [9]Department of Rheumatology and Inflammation Research, University of Gothenburg, Gothenburg, Sweden; [10]Division of Inflammation and Infection, Department of Biomedical and Clinical Sciences, Linköping University, Linköping, Sweden; [11]Department of Pharmacological and Technological Chemistry, I.M. Sechenov First Moscow State Medical University, Moscow, Russia; [12]Division of Rheumatology, University Hospital Frankfurt, Goethe University, Frankfurt am Main, Germany.

*A. Coelho, A. Krämer, and A. Saxena contributed equally to this paper. Correspondence to Rikard Holmdahl: rikard.holmdahl@ki.se.

et al., 2016) and is expressed in the thymus (Raposo et al., 2018) and BM, hence COL2 is a prime example for a tissue-specific protein providing a scaffold for the selection of the immune system.

Since the C1 epitope on the COL2 triple helical molecule (aa 359–370) in mice and humans is identified as a major epitope in CIA and RA (Burkhardt et al., 2002; Uysal et al., 2009; Viljanen et al., 2020) and is recognized by germline-encoded antibodies (Mo et al., 1993), we sought to molecularly define and functionally characterize their precursor C1-specific B cells (C1-B) in both healthy mice and humans. Using unique triple-helical peptide (THP) C1-streptavidin tetramers, C1-B were tracked across species and the cloning and expression of their germline-encoded B cell receptor (BCR) corroborated their specificity to the C1 epitope. Single-cell sequencing (scRNA-seq) analysis revealed an antigen processing and presentation signature as well as the upregulation of surface markers, such as chemokine receptor 7 (CCR7) and the inhibitory surface protein CD72 in C1-B. We demonstrated that C1-B have a potent suppressor function in protecting against arthritis. The suppressor effect was found to be independent of IL10 secretion, dissociating them from earlier described B10 cells (Dilillo et al., 2010; Tedder, 2015). Disease suppression correlated with the induction of COL2-reactive regulatory T cells (Tregs) by C1-B and was deemed to be mediated by CD72, an inhibitory C-type lectin expressed by naïve B cells. These results propose a defined novel population of epitope-specific autoreactive B cells which could be a key for understanding immune tolerance.

Results

Detection of COL2-specific B cells in mice, rats, and humans

Anti-C1 antibody response detected in mice immunized with COL2 signals the existence of autoreactive B cells since these antibodies target conserved epitopes on COL2. Intriguingly, almost all cloned COL2-specific B cells, including those secreting anti-C1 antibodies, bind their epitopes only in a triple helical format, owing to the physiological structure of COL2 (Fidler et al., 2018), and the antibodies bind joint cartilage in vivo (Mo et al., 1994). Hitherto, we successfully synthesized THP of defined B cell epitopes on COL2 (Viljanen et al., 2020). We then mounted tetramers consisting of an R-phycoerythrin (PE)–labeled streptavidin core and four biotinylated C1 THP and a control triple helical peptide with glycine/proline/hydroxyproline repeats but lacks the C1 epitope (glycine proline hydroxyproline [GPO]; Fig. 1, A and B). Within the B cell population, we observed a minor population of C1-B in the spleen and BM. To increase the frequency and enumerate these cells, we applied an enrichment method previously used to detect antigen-specific B cells (Pape et al., 2011). Thus, C1-B were enriched from spleens and BMs of mice, rats, and humans (healthy and RA) using paramagnetic beads and different tetramer constructs to limit unspecific binding (Fig. 1 C and Fig. S1, A–C). We found a surprisingly high and distinct number of C1-B in the spleen (1 in 10^4 B cells) and BM (1 in 10^5 B cells) of mice and rats, and in peripheral blood mononuclear cells (PBMCs) from healthy humans (1 in 10^5 B cells; Fig. S1 D). Compared with healthy donors (HD), RA individuals displayed an eightfold decrease in the ratio of C1-specific/polyreactive B cells but with an increase in C1-specific antibodies in RA patients (Fig. S1, E and F). Because B cell central selection occurs primarily in the BM, we asked whether COL2 and specifically the C1-epitope are exposed in the BM. A specific COL2 staining was found on cartilaginous trabeculae in the BM of neonatal and adult mice shown here by in vivo binding of a C1-specific monoclonal antibody (mAb), CB20 (Karlsson et al., 1995; Fig. 1 D). To validate the enrichment and staining of C1-B, we cloned and recombinantly expressed four antibodies (Table 1) from single-sorted C1-B derived from human PBMCs (Fig. S1 G). We then tested the specificity of the mAbs MAK1, 4, 5, and 6 by two different approaches. All MAK antibodies showed a high specificity to the C1-epitope. Only two out of the four antibodies (MAK5 and 6) bound the full COL2 protein and none of them displayed any reactivity against control peptides and proteins (streptavidin-PE, GPO, and modified C1-epitope; Fig. 1 E). To verify whether MAK antibodies bind other known epitopes on COL2, we subjected them to a multiplex bead-based assay that comprises the major COL2 epitopes of different structures (triple helical "T" vs. cyclic "C") and modification (arginine to citrulline or lysine to homocitrulline/hydroxylysine). Bead-based immunoassay revealed high specificity of MAK antibodies against only the native THP C1-epitope containing two arginine residues, thereby denoted "C1-R-R" (Fig. 1 F).

Taken together, these data imply that autoreactive epitope-specific B cells populate the B cell repertoire of the mammalian species tested, and we then examined whether COL2-specific B cells are positively or negatively selected.

COL2-specific B cells bypass all mechanisms of negative selection

To date, three mechanisms of negative selection have been described with the onus of purging autoreactive B cells. We investigated whether C1-B undergo clonal deletion, receptor editing, and/or anergy since they are considered autoreactive cells. Assessed by a panel of lineage-specific surface markers, we stained spleens and BM-enriched cells from wild type BQ ($C57BL/10.A^q$) mice. We observed C1-B, at different frequencies and numbers, in each population investigated (immature, transitional, marginal zone, and follicular B cells; Fig. 2 A and Fig. S2 A). To estimate the median affinity of C1-B for the C1 peptide ex vivo, we utilized an already validated flow cytometric assay (Taylor et al., 2012) on cells isolated from the ACB (anti-C1 B) mice (Cao et al., 2011; Khmaladze et al., 2015). ACB mice are knock-in for the CB20 heavy chain only (Fig. S2 B), which allows physiological recombination with a light chain of sufficient affinity for the C1 epitope. Splenocytes from naïve ACB mice were preincubated with increasing concentrations of C1 or GPO THP and an irrelevant protein (ovalbumin) before C1-tetramer labeling. The frequency of C1-B was displayed as a percentage relative to the control sample (stained with only the C1-tetramer without preincubation). C1-B did not bind GPO THP; almost 100% of the C1-B could be retrieved even after incubation with high GPO THP concentration (322 pM–32.22 µM range). In contrast, incubation with ∼1 µM of C1 THP was sufficient to

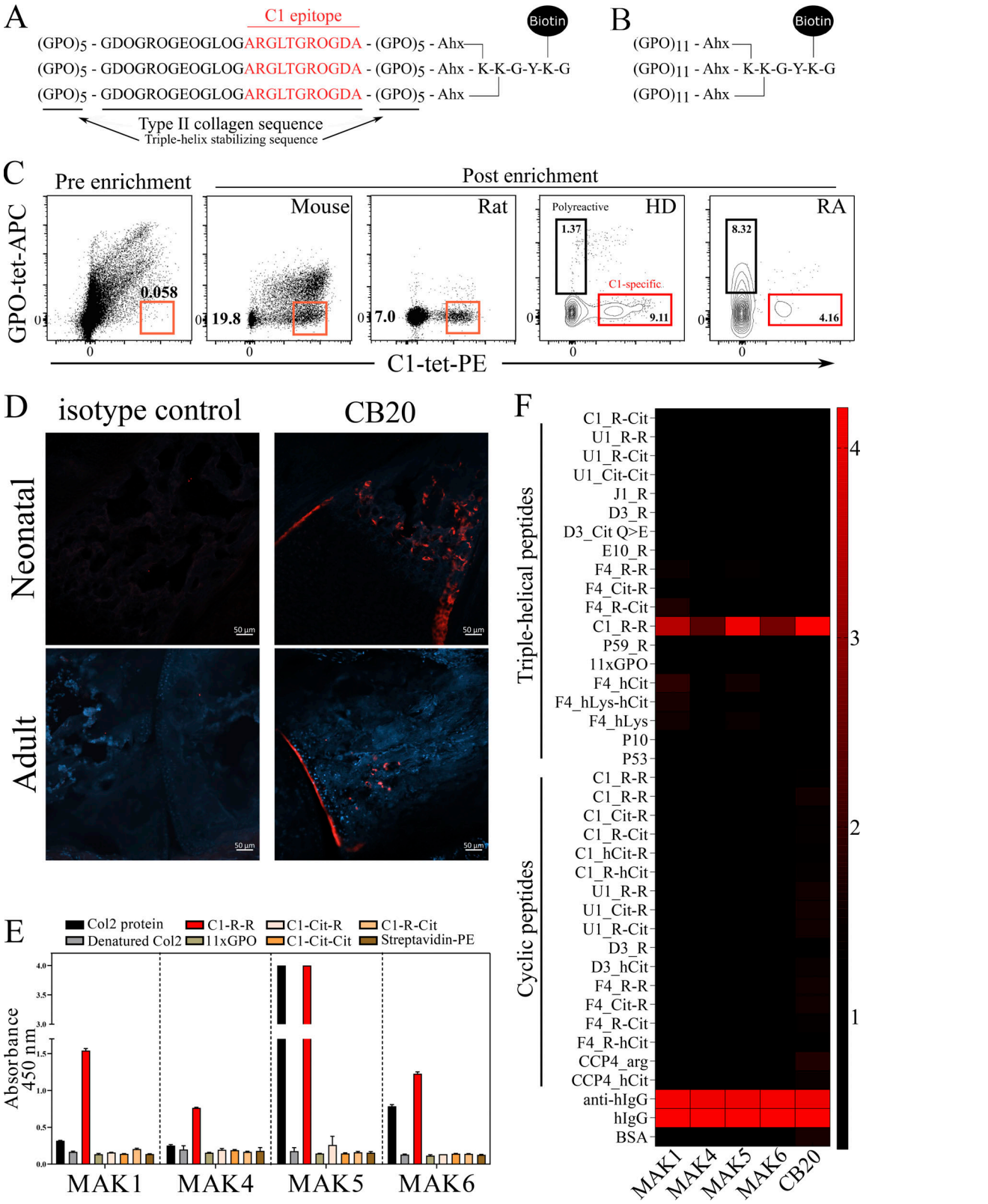

Figure 1. **Collagen-reactive C1-B are naturally detected in mice, rats, and humans. (A and B)** Schematic design of the synthesized triple helical C1 tetramer and GPO control tetramer. **(C)** Representative flow cytometry plots depicting the frequency of C1-B from pooled spleens before enrichment in mice and following post-enrichment protocol in mice, rats, and PBMCs of HD and RA samples. **(D)** Ex vivo visualization of the C1-epitope using CB20 antibodies on cryofixed joint tissues of neonatal (upper panel) and adult mice (lower panel), revealing the exposure of the C1 epitope in the BM trabeculae. **(E)** Binding of five unique anti-C1 clones (MAK1, 4, 5, and 6) assessed by ELISA. **(F)** Binding of MAK antibodies to other defined COL2 epitope libraries assessed by bead-based multiplex assay. Error bars represent mean ± SEM. Scale bars are 50 µm.

Table 1. **MAK antibody sequences**

Clone	V gene	D gene	J gene	CDR3	Germline (%)
MAK1	IGHV4-59*01	IGHD6-19*01	IGHJ4*02	ARRGEQWGDGDWFDP	99
	IGKV1-39*01		IGKJ1*01	QQSYSHPWT	99.6
MAK4	IGHV4-34*01	IGHD6-19*01	IGHJ4*02	ARGGIAVAGAEPFDY	99.7
	IGKV1-33*01		IGKJ3*01	QQYDNLPPT	100
MAK5	IGHV3-21*01	IGHD3-22*01	IGHJ4*02	GGDYDSSGLFEY	99.3
	IGKV1-5*01		IGKJ1*01	QQYNSYSWT	100
MAK6	IGHV3-11*01	IGHD1-26*01	IGHJ4*02	ARGGGELLDY	100
	IGKV1-39*01		IGKJ2*01	QQSYSTPYT	100

reduce the number of retrieved C1-B cells by 50% (Fig. S2, C and D). IC_{50} values reflect a relatively weak binding of the C1-specific BCR to its cognate peptide as compared with somatically mutated antibodies (Karlsson et al., 1995) and provide a rationale for the persistence of these cells.

However, affinity measured in vitro might not reflect the more relevant interaction in vivo. Clearly, the CB20 antibody binds rapidly and sustainably to the BM matrix, as illustrated by immunohistochemical staining of joints from CB20-injected neonatal mice (Fig. 1 D), indicating that B cells with the same receptor could also interact with COL2.

To explore whether C1-B undergo receptor editing, we isolated proteins from freshly sorted $C1^+$ and $C1^-$ B cells (C1-tetramer positive vs. C1-tetramer negative cells) from ACB mice and quantified protein expression by mass spectrometry–based proteomics. Interestingly, the most highly expressed protein in the C1-B fraction corresponded to the immunoglobulin kappa chain variable 3 family (Igkv3-7), which is the V gene used by the CB20 antibody (Cao et al., 2011; Fig. 2 B). This shows that C1-B ignore receptor editing as the light chain that recombines with the heavy chain knock-in corresponds to the original CB20 clone. Moreover, we analyzed the remaining differentially expressed proteins at steady state and found that most of the downregulated proteins in C1 positive compared with C1 negative B cells (Fig. 2 B and Fig. S2 E) consisted of ribosomal subunits (40S and 60S proteins).

Next, to assess the state of C1-B, we evaluated their functional properties in terms of antigen processing and presentation. As native COL2 is a high molecular weight fibrillar triple helical molecule, it needs to be internalized and processed before it can be presented to T cells. We found that naïve B cells from ACB mice, incubated with native COL2, efficiently activated COL2-reactive HCQ3 T cells, i.e., naïve transgenic T cells specific for the major 259–270 galactosylated peptide on COL2 (Raposo et al., 2018), denoted here as Gal or Gal-COL2 (Fig. 2 C). We did not notice differences in the level of IL2 production when the relevant COL2 peptide was used, as there is no need for processing a peptide that can be loaded directly onto major histocompatibility complex type II (MHCII) molecules (Fig. 2 D). Furthermore, in vivo COL2-pulsed B cells from ACB mice activated COL2-specific T cells ex vivo without the addition of exogenous antigen (Fig. 2 E). Lastly, formalin-fixed B cells failed to trigger any T cell responses in the presence of COL2, owing to the need for processing by live cells (Fig. 2 F).

The native C1-epitope (aa 359–370) harbors two arginine residues in each alpha chain building the triple helical molecule (Fig. 1 A). A mutation from arginine to glutamine at position 360 ($COL2^{R360Q}$) abrogates the binding of the CB20 to the C1 epitope (Fig. 2 G) but could still engage a polyclonal response to the C1 epitope (Fig. S2 F). To test the repercussion of that mutation on C1-B, we engineered a mouse that expresses the $COL2^{R360Q}$ epitope on its native COL2 and crossed it to the ACB mouse, thereby denoted as ACB.$Col2^{R360Q}$. We observed a reduction in frequency and absolute number of C1-B in the LNs and spleens of BQ.$Col2^{360Q}$ and ACB.$Col2^{360Q}$ mice as compared with $Col2^{R360}$ littermates (Fig. 2, H and I; and Fig. S2, G and H). Surprisingly, we did not detect significant changes in the frequency and absolute number of C1-B in the BM of ACB.$Col2^{R360Q}$ as compared with ACB. However, V_κ gene sequencing of BM B cells revealed an increased frequency of mutations in the CDR3 region (position 116 on the Light chain) in ACB.$Col2^{R360Q}$ mice and altered Igkv3 usage between ACB.$Col2^{R360Q}$ and ACB mice (Fig. S2, J and K).

Altogether, these data demonstrate that C1-B bypass all known mechanisms of negative selection, such as clonal deletion, receptor editing, and anergy. Instead, we provide evidence that native COL2, in both BM and LNs, selects C1-B, which intrigued us to examine their role in mouse models of autoimmunity.

C1-B suppress antigen-specific inflammation independently of IL10

To address the functional role of C1-B in vivo, we employed established mouse models of autoimmunity, CIA, and experimental autoimmune encephalomyelitis (EAE). We primarily adopted recipient mice with a mutation in the *Ncf1* gene on the B10Q background (BQ.$Ncf1^{m1j}$) that enhances susceptibility to autoimmune diseases in rodents and humans (Hultqvist et al., 2004; Olsson et al., 2017; Zhao et al., 2017). Adoptive transfer of naïve B cells from ACB mice into syngeneic BQ.$Ncf1^{m1j}$, before COL2 immunization, stunted the development of arthritis (Fig. 3 A and Fig. S3 A). Joint histology (Fig. 3 B), quantified with inflammation score (Fig. 3 C), and antibody response (Fig. S3 B) in recipient mice confirmed the suppressive role of C1-B.

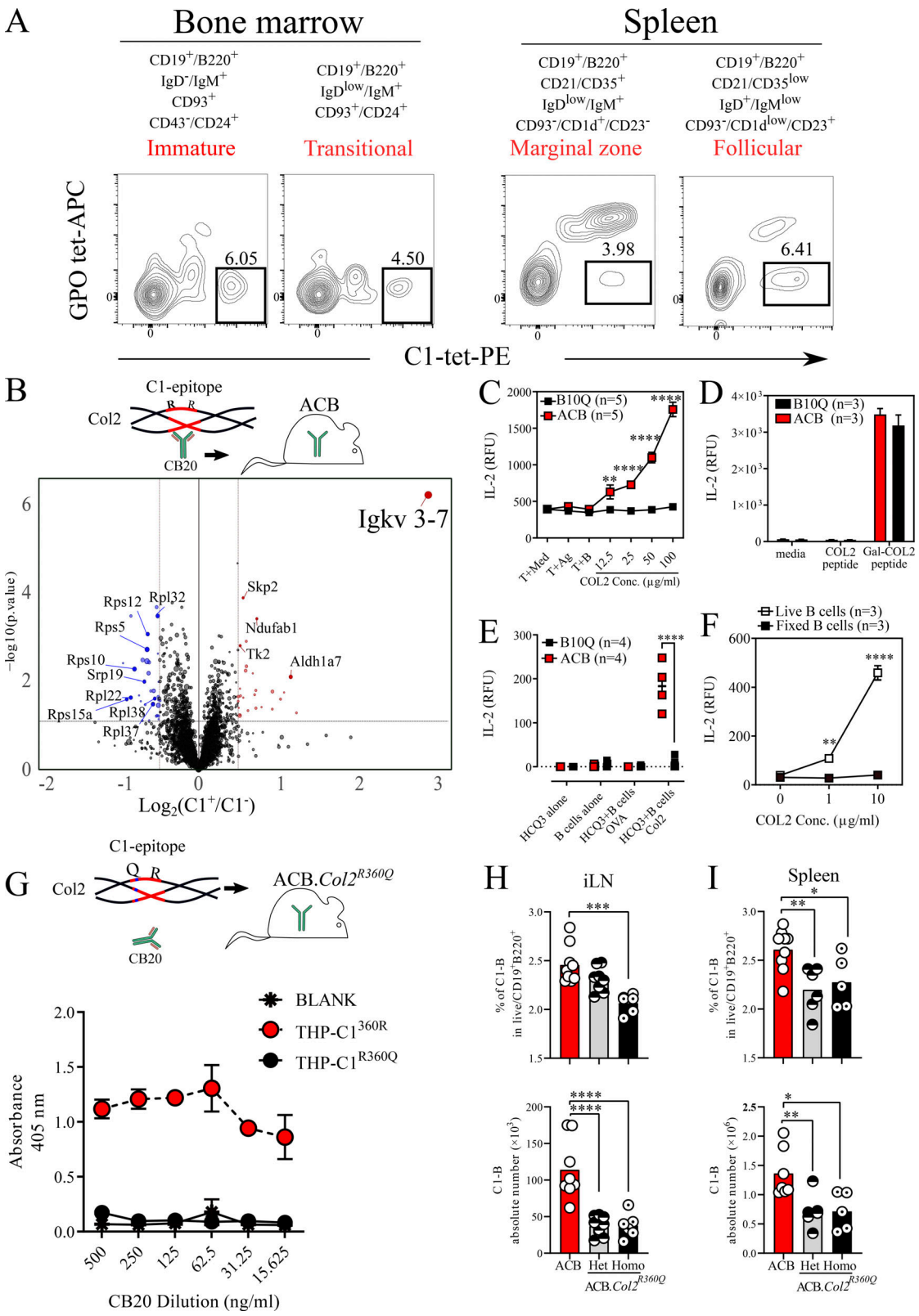

Figure 2. **C1-B bypass mechanisms of negative selection. (A)** Frequency of persistent C1-B in the BM and spleen of wild-type mice (n = 5 pooled). **(B)** Mass spectrometry–based proteomic analysis of sorted C1-B from heavy chain CB20 knock-in (green) ACB mice. Light chain Igkv 3–7 was the most significantly upregulated protein in C1-B compared to the rest of B cells (n = 5 mice/group). **(C)** IL2 titers from the supernatants were assessed by ELISA after co-culture of COL2-reactive T cell hybridoma together with purified B cells from LN of ACB mice with or without COL2. **(D)** Like C, but cells were cultured in the presence of MHCII-restricted COL2 peptide (gal-COL2) recognized by the T cell hybridoma. **(E)** In vivo COL2-pulsed B cells with either ovalbumin or COL2, purified, and co-cultured with T cell hybridoma without the addition of exogenous antigens. IL2 titers were assessed by ELISA 24 h later. **(F)** Like in C, but B cells were either

fixed with formaldehyde or maintained live. **(G)** ACB.*Col2*^{R360Q} mouse expresses a mutated COL2 protein at the C1-epitope, point mutation Q–R, leading to the abrogation of CB20 binding to the mutated epitope. **(H and I)** Frequency and absolute number of C1-B in ACB, heterozygous, and homozygous ACB.*Col2*^{R360Q} LN and spleens (n = 5–8 mice/group). Error bars represent mean ± SEM. Statistical significance was determined using two-way ANOVA followed by Sidak's test. *P < 0.05, **P < 0.01, ***P < 0.001, and ****P < 0.0001.

In contrast, C1-B from ACB mice failed to inhibit EAE demonstrating the antigen specificity of the suppressive effect (Fig. 3 D). Because C1-B produce IL10 upon stimulation (Fig. S3, C and D), we anticipated a role for IL10 in mediating arthritis suppression as a consensus exists around the indispensability of IL10 in mediating the role of regulatory B cells (B10 cells; Mauri et al., 2003; Hu et al., 2006). To our surprise, the adoptive transfer of naïve B cells from IL10 deficient (IL10$^{-/-}$) ACB and BQ mice into the susceptible host still maintained a suppressive phenotype even in the absence of IL10 (Fig. 3 E). Joint histology, inflammation score, and antibody response confirmed the suppressive effect of C1-B independent of IL10 (Fig. 3, F and G; and Fig. S3 E). Despite the strong suppression achieved by ACB B cells, C1-B represent only ∼5% of the B cell repertoire (Fig. S3 F). To decisively attribute the suppressive effect to the C1-B population, we sorted naïve B cells and magnetically enriched C1-specific cells from ACB mice, where 75% of sorted B cells were C1^{+} (Fig. S3 G), and adoptively transferred 2–5 × 10^{5} cells into each BQ.*Ncf1*^{m1j} mouse. In parallel, the same number of naïve B cells from BQ mice were transferred to each BQ.*Ncf1*^{m1j} mouse. Even with the limited number of transferred cells, C1-B successfully suppressed arthritis exhibited by a lower clinical score (Fig. 3 H) and diminished pathogenic IgG2b antibody response against COL2 or C1 epitope (Fig. 3, I and J). Additionally, the transferred C1^{+} and C1^{-} B cells from the ACB mice and B cells from BQ mice into QD mice (Nandakumar et al., 2003; BQ X DBA/1) F1 cross did confirm the specific suppressive function of C1-B (Fig. S3 H). Of note, the transfer of C1-B after immunization after 10 or 70 d failed to confer any clinical response as shown in Fig. S3 (I and J) and Fig. 3 H (arrow).

Besides the suppression of clinical arthritis, C1-B recipient mice displayed an increase in the frequency of activated Tregs (CD44^{high}Foxp3^{+}; Fig. 3 K) analyzed from joint draining LNs. Moreover, the proliferation of antigen-experienced Tregs could be reproduced when LNs from recipient mice were maintained in culture in the presence of the cognate antigen and the survival cytokine, IL2 (Fig. 3, L and M).

Collectively, these results confirm the potent suppressive effects of C1-B distinct from the conventional "B10" as they operate independently of IL10.

Antigen-presenting C1-B induce COL2-specific Treg proliferation in a contact-dependent manner

The increased frequency, activation, and proliferation of polyclonal Tregs, comprising both Tregs (FOXP3^{+}) and Tr1 (Gagliani et al., 2013; CD49b^{+}LAG3^{+}) population, repeatedly observed in COL2-immunized ACB mice (Fig. 4, A–E) prompted us to investigate closely the functional capacity of C1-B in tolerizing T cells. To convincingly attribute this regulation to C1-B, we gauged T cell responses in ACB.*Col2*^{R360Q} mice because of the reduction in the numbers of C1-B in the secondary lymphoid organs (Fig. 2, H and I) while retaining a physiological B cell repertoire. The analysis of COL2-specific Vβ8.3^{+} T cells in ex vivo cultured LNs cells derived from naïve ACB and homo/het ACB.*Col2*^{R360Q} mice confirmed the role of C1-B in controlling the proliferation (Ki67^{+}) and activation (CD44^{+}) of COL2-specific Tregs (Fig. 4, F–H). In a supplementary experiment, co-culture of B cells from ACB and ACB.C1^{R360Q} mice together with transgenic primary T cells specific for the native COL2$^{259–270}$ peptide (QC) cells (Brand et al., 2002) reproduced the reduced proliferation and activation of COL2-specific Tregs (Fig. S4, A–D).

As a substitution to the heavy chain knock-in C1-B from the ACB mouse, and since we were hesitant to whether GPO-C1 cross-reactive population found in WT mice (Figs. 1 C and 2 A) could match the antigen-presenting activity of C1-B, we assessed natural C1-B from naïve BQ mice. Thus, we sorted 1 × 10^{4} C1-B, GPO-C1 cross-reactive, and double negative B cells by FACS from BQ mice and cultured them with QC cells. Macrophages with and without lipopolysaccharide activation were used as an additional control (Fig. S4 E). The elevated frequency and activation threshold of Tregs co-cultured with natural C1-B proved their distinctive capacity in inducing and activating Tregs (Fig. S4, F and G).

To gain insight into how natural C1-B triggers the expansion of antigen-specific Tregs, we assessed whether the nature of this interaction requires a physical interaction between both cells. To this end, we applied a transwell system where enriched C1-B or B cells from BQ mice, in the presence of COL2 as a cognate antigen, were placed together with ex vivo–purified primary COL2-specific T cells in one chamber (contact-dependent) or separated from QC cells by the transwell insert (contact independent; Fig. 4 I). Despite the ability of C1-B in secreting IL10 (Fig. S3 C), we failed to detect a prominent proliferation of Tregs in the contactless set-up. In fact, the cognate interaction between C1-B and QC cells was necessary to trigger a potent proliferation of Tregs only in the presence of COL2 (Fig. 4, J and K).

The prevalence of a B1 subset of C1-B in the peritoneal cavity has been described (Cao et al., 2011) but their role in Tregs induction was never tested. Coculture of enriched C1^{+} B cells from peritoneal exudate cells of ACB mice with purified QC T cells induced the activation of Tregs in the presence of COL2 when compared with controls (Fig. S4 H).

These results establish the antigen processing and presentation aptitude of natural autoreactive B cells and their function in triggering the proliferation of Tregs in the presence of the cognate antigen and in a contact-dependent manner.

C1-B hold an antigen presentation signature and upregulate CCR7 and CD72 upon activation

While we showed that autoreactive C1-B exist in mice and men and on the transcriptional level mouse and human gene profiles are overall conserved, we chose to define the more relevant C1-B from HD by transcriptomics to later validate the hits in the

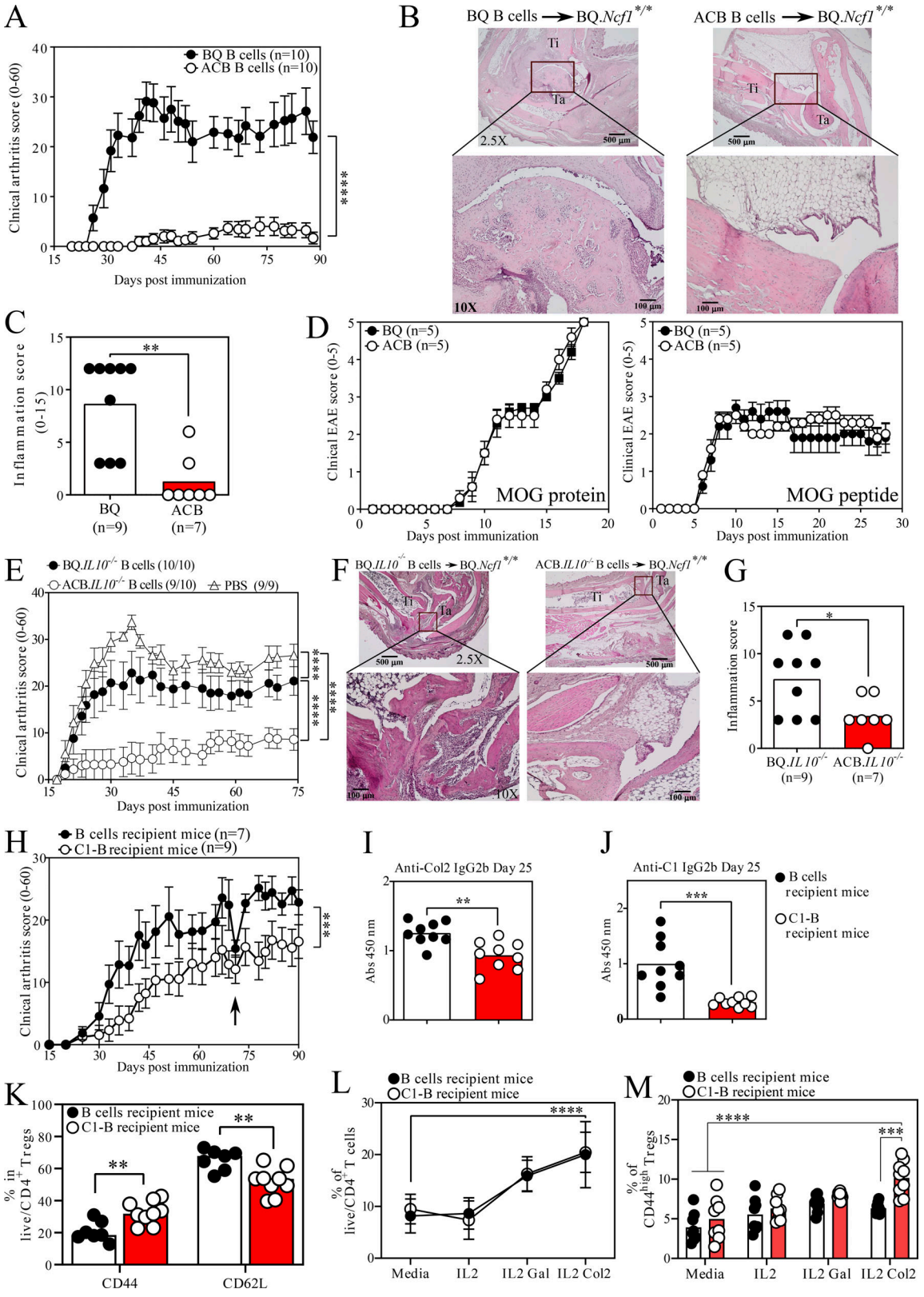

Figure 3. **C1-B suppress tissue-specific inflammation independent of IL10. (A–C)** Adoptive transfer of naïve B cells from ACB and BQ mice into syngeneic autoimmune-prone BQ.*Ncf1*^{m1j} recipient. Arthritis clinical score, representative histological H&E staining of tibia (Ti) and talus (Ta), and histopathological assessment in recipient mice. **(D)** EAE clinical score in ACB and BQ mice after MOG protein and MOG peptide immunization. **(E–G)** Adoptive transfer of naïve B cells from ACB.*IL10*$^{-/-}$, BQ.*IL10*$^{-/-}$ mice or no transfer (PBS) into syngeneic autoimmune-prone BQ.*Ncf1*^{m1j} recipient. Arthritis clinical score, representative histological H&E staining of tibia (Ti) and talus (Ta), and histopathological assessment in recipient mice. **(H)** Arthritis score of syngeneic autoimmune-prone BQ.*Ncf1*^{m1j} recipient mice after adoptive transfer of 0.5 × 10^6 C1-B or B cells. **(I and J)** Serum titers of anti-COL2 and anti-C1 IgG2b antibody in recipient mice of

H 25 d after immunization was assessed by ELISA. **(K)** Frequency of CD44$^+$ and CD62L$^+$ Tregs (Foxp3) in the LNs of recipient mice of H 90 d after immunization. **(L and M)** In vitro recall assay of LNs derived from H depicting Tregs proliferation and activation after 48 h of culture with different antigens. Error bars represent mean ± SEM. Statistics in A, C, E, and G–K were determined by two-tailed Mann–Whitney *U* test. Significance in L and M was determined by two-way ANOVA followed by Sidak's test. *P < 0.05, **P < 0.01, ***P < 0.001, and ****P < 0.0001. Scale bar for 2.5× is 500 µm and for 10× is 100 µm.

mouse. Thereby, we single-cell sorted C1-B, GPO-specific, and double negative for C1$^-$/GPO$^-$ B cells from three human HD and subjected the cells to sequencing using the smart-seq3 approach. B cells were analyzed with *t*-distributed stochastic neighbor embedding for dimensionality reduction and that revealed principal partitioning into three distinct clusters (Fig. 5 A). The sorted B cell populations were equally distributed along the demarcated clusters (Fig. 5 B) that grouped different subsets of B cells according to their state. Derived from the expression of *CD27*, *IGHM*, *IGHD*, and *MS4A1*(*CD20*), we delineated CD27^{high}CD20^{high}IGD^{low} memory cells (cluster 1), CD27^{low}CD20^{high}IGD^{high} naïve cells (cluster 2), and CD27^{low}CD20^{low}IGD^{low} B cells (cluster 3; Fig. 5 C). To navigate through the list of differentially regulated genes provided by scRNA-seq (Fig. S5 A), we narrowed it down to certain immune-related genes that either were significantly regulated, such as *CCR7*, *CXCR4*, and *VEGFB*, or belonged to the top 50 genes according to fold change such as *CD72* and *IL4R* (Fig. 5 D). Gene set enrichment analysis between C1$^-$- and GPO$^-$-specific B cells revealed a signature in MHCII peptide assembly, chemokine receptor activity, and ribosomal subunits (Fig. 5 E). Flow cytometry validated the increased surface expression of MHCII on naïve spleen and BM-derived C1-B, hinting at a superior antigen presentation capability (Fig. 5, F and G). We also investigated kinetically the upregulation of CCR7 on peripheral blood C1-B following COL2 immunization in ACB and BQ mice. Steadily, CCR7 expression continued to increase peaking at day 10 after immunization in C1-B (Fig. 5 H). This was mirrored by the progressive upregulation in CCR7 surface expression on circulating C1-B from ACB and BQ mice (Fig. 5, I and J). To better delineate the C1-B population, we immunophenotyped LN-derived cells from BQ mice 30 d after COL2 immunization (Fig. 5 K). Only the gated C1-B population co-expressed both CCR7 and CD72 (Fig. 5 L).

We then questioned whether the co-expression of CCR7 and CD72 is unique to autoreactive B cells. Therefore, we compared PE-specific B cells following PE immunization, as a model for non-self-antigen specificity, to C1-B following COL2 immunization in BQ mice. After PE and C1 enrichment, respectively, we detected the upregulation of CCR7 and CD72 only in C1-B (Fig. S5, B and C). Interestingly, C1-B retained a naïve phenotype characterized by a high IgM and IgD expression even 10 d after COL2 immunization in contrast to the isotype-switched PE-specific B cells (Fig. S5, D and E). In humans, IgG$^-$ C1-B exhibited the highest expression of surface CD72 as compared with IgG$^+$ B cells and IgG$^-$ B cells (Fig. S5 F).

Thus, in line with transcriptome data, we define C1-B as antigen-presenting cells that upregulated the dual expression of CD72 and CCR7 following activation with the cognate antigen.

Blocking CD72 on C1-B impedes COL2-specific Tregs induction

Evidently, the upregulation of CCR7 on activated C1-B suited their profile as it is known to drive the chemotaxis of APC, including B cells, to the LNs for T cell priming (Ohl et al., 2004), yet an explanation for CD72 expression remained unresolved. To flesh out a function for the BCR co-receptor CD72 on C1-B, we crossed ACB to QC mice (ACB.QC) and cultured splenocytes in the presence of a CD72 blocker (anti-CD72) or an isotype IgG1 control. Blocking CD72 did result in a decrease in the frequency of proliferating Tregs, while no change in frequency was detected in the presence of the isotype control (Fig. 6, A and B). To substantiate the in vitro culture, we immunized ACB mice with COL2 and injected half of the mice with a single 50 µg dose of anti-CD72 antibody 7 d later (Fig. 6 C). Despite the unnoticeable differences among the proliferating Tregs 7 d after treatment, it was clear that mice injected with anti-CD72 antibody accumulated more Tregs that failed to proliferate when compared with the control group (Fig. 6, D and E). This was accompanied by an elevation in the frequency of circulating B cells (Fig. 6 F) that connected it to the increased anti-COL2 and anti-C1 antibody serum levels from the anti-CD72 group (Fig. 6, G and H). Although ACB mice are completely resistant to CIA, anti-CD72 injections were sufficient to break the strong tolerance maintained by C1-B in 50% of the treated mice (Fig. 6, I and J). Representative histological slides corroborate the joint inflammation, lymphocyte infiltration, and synovial destruction in ACB mice treated with anti-CD72 (Fig. 6 K).

We then hypothesized that a decrease in CD72 expression on C1-B would result in a similar phenotype. To achieve that, we cultured C1-B in the presence of IL4 since it has been shown to reduce the expression of CD72, among other inhibitory proteins (Rudge et al., 2002). Indeed, the addition of IL4 to the culture media reduced the expression of surface CD72 on C1-B (Fig. 7, A and B). This reduction in CD72 expression correlated with the decreased efficiency of C1-B in inducing the proliferation and activation of Tregs when IL4 was added to the mix (Fig. 7, C and D). Because other co-stimulatory molecules, such as CD86, have been shown to be important in regulating T/B interactions (O'Neill et al., 2007), we tested its significance in our model. Blocking CD86 with a specific mAb did not influence the proliferation and activation of Tregs by C1-B when compared with anti-CD72 treatment (Fig. 7, E and F). In fact, treatment with anti-CD72 blocked the receptor on the surface of C1-B and did not induce its internalization, validated using different anti-CD72 mAb clones (Fig. 7 G). Also treating C1-B cells with anti-CD72 did not induce any major changes in activation markers (CD44/CD69), in antigen presentation-related proteins (MHCII/CD86), and in chemotaxis-related receptors (CXCR5/CXCR4; Fig. 7 H).

CD72 expression is not restricted only to B cells, hence obscuring the specific C1-B effect observed in ACB mice treated with intravenous injection of anti-CD72. We chose to enrich C1-B from ACB mice and pretreat them ex vivo with anti-CD72 or an isotype control before adoptively transferring them back to

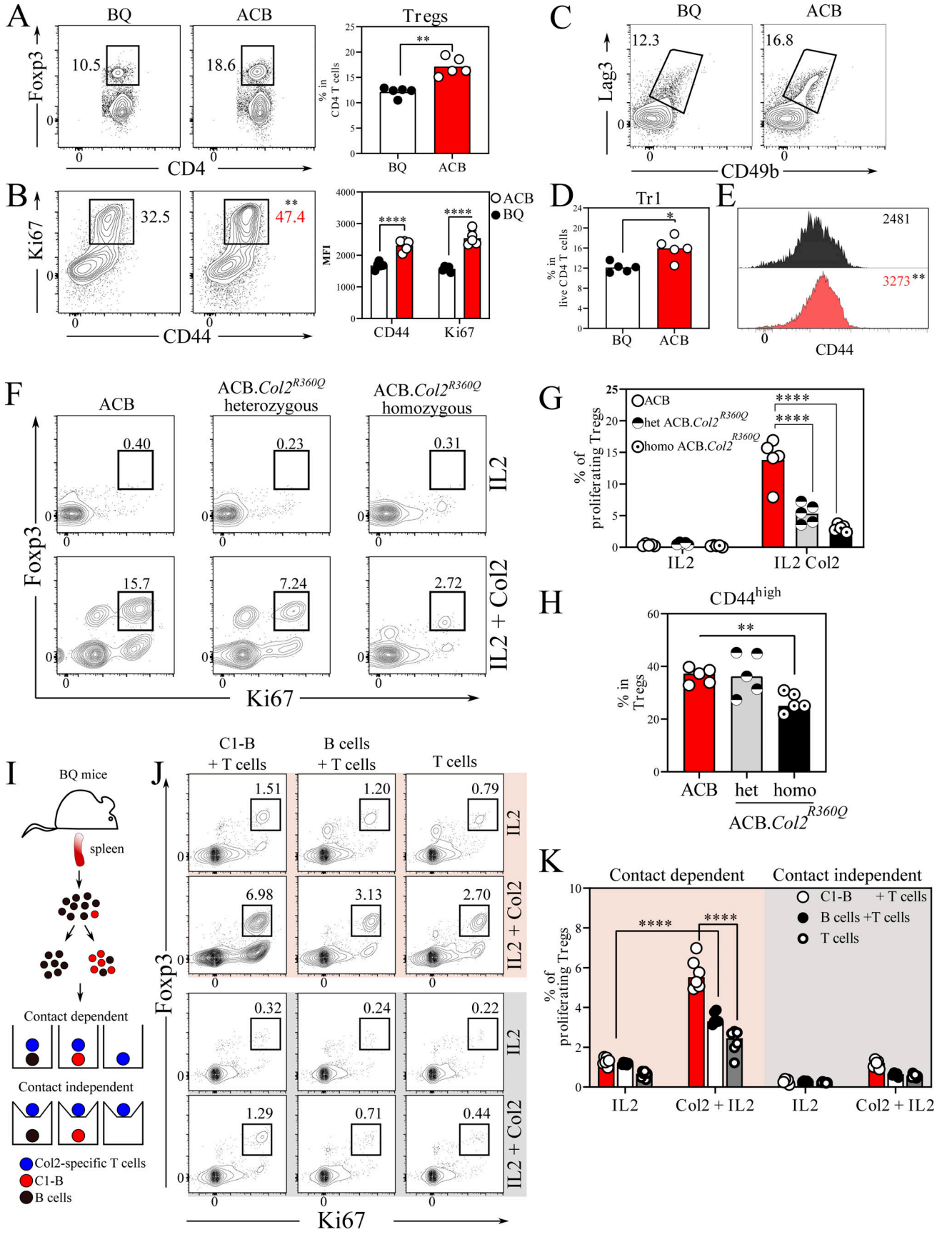

Figure 4. **C1-B are potent inducers of Tregs. (A and B)** Frequency, activation, and proliferation of FOXP3⁺ Tregs in the LNs of 10 d immunized ACB and BQ mice (n = 5 mice/group). **(C–E)** Frequency and activation of LAG3⁺CD49b⁺ Tr1 cells in the LNs of 10 d immunized ACB and BQ. **(F and G)** Flow cytometry plots

depicting the frequency of endogenous COL2-reactive Vβ8.3 proliferating Tregs (FOXP3⁺Ki67⁺) after in vitro culture of LN cells derived from ACB, heterozygous and homozygous ACB.*Col2*^{R360Q} mice (n = 5 mice/group). **(H)** Frequency of CD44⁺ Tregs gated on F. **(I)** Experimental setup for contact-dependent and independent Treg induction experiment. **(J and K)** Flow cytometry plots depicting the frequency of proliferating Tregs in direct contact (pink), contactless (gray) culture alone or with natural C1-B and B cells purified from BQ mice in the presence or absence of COL2 (n = 18 mice, each symbol represents three mice pooled). Error bars represent mean ± SEM. Statistics in A, B, D, and E were determined by two-tailed Mann–Whitney U test. Significance in G, H, and K was determined by two-way ANOVA followed by Sidak's test. ****P < 0.0001.

BQ.*Ncf1*^{m1j}. Arthritis observed in anti-CD72 treated C1-B recipient mice matched the PBS group while arthritis incidence and severity were significantly reduced in the isotype control-treated C1-B recipient mice (Fig. 7 I). COL2-antibody response mimicked the disease phenotype and C1-antibody response validated the transfer of C1-B when compared with the PBS control group (Fig. 7 J). Phenotypic characterization of transferred C1-B revealed that the disease suppression was mediated by follicular and marginal zone origin based on CD23 and CD21/35 expression, albeit at different frequencies (~80 to ~20). These cells did not upregulate conventional inhibitory markers that have been previously shown to possess suppressive functions such as TIM-1 (Shankar et al., 2022), CD5, and CD1d, although, as expected, marginal zone C1-B cells exhibited higher expression of CD1d compared with follicular C1-B (Fig. 7 K).

Discussion

The identification of antigen-specific B suppressor cells fills a gap in the understanding of immune selection and tolerance. We suggest that antigen-specific B cells with suppressive functions are positively selected on a limited set of epitopes on proteins expressed both centrally (BM) and peripherally (cartilage, with drainage to lymphoid organs) and mediate their suppressor functions mainly through activation of Tregs, selected on the same protein expressed in the thymus. Earlier seminal studies neatly spawned the mechanisms that define B cell negative selection (Holmdahl et al., 1986; Goodnow et al., 1988; Nemazee and Bürki, 1989), yet these reports relied on two main anchors to investigate B cell tolerance; double transgenic mice that expressed (1) ubiquitous cell-surface or soluble artificial self-antigens and (2) high affinity (picomolar range) BCR heavy/light chain to the cognate antigen. Here, particular interest is focused on the physiologic expression of a germline-encoded heavy chain BCR and a tissue-restricted, RA-associated, self-antigen such as COL2. Applying this model, we uncovered a bona fide population of autoreactive B cells that bypass mechanisms of negative selection, egress from the BM, and populate the periphery. The role of these antigen-specific B cells is to activate antigen-specific Tregs and subsequently suppress tissue-specific inflammation. Mechanistically, the suppressive function of these B cells is mediated, in part, by CD72 since its blockade affected Treg induction, antibody response, and disease susceptibility (Fig. 6). The number of C1-B are decreased in RA and instead potentially pathogenic antibodies to the C1 epitope are produced implicating the importance of hindering C1-B from differentiating to plasma cells.

The discovery that COL2-specific B cells ignore negative selection motivated us to rethink the dogma behind B cell selection. Although T cell–independent positive selection of B cells has been described (Chen et al., 2022), these studies relied solely on BCR repertoire analysis to circumvent the absence of a relevant autoantigen. Repetitive motifs can drive the activation of poly/autoreactive B cells (Csomos et al., 2022), often associated with autoimmunity (Cancro, 2020). In fact, COL2 is a prime archetype of a protein with repetitive motifs as its structure consists of three identical α chains harboring the triple-helix stabilizing GPO repeats across the entire protein. This effect is amplified in vivo since fibril-forming COL2 occupies densely different tissues. The necessity for an exposed native C1 epitope highlighted in the ACB.*Col2*^{R360Q} mouse strain provides tentative evidence for positive selection of a much-needed autoreactive C1-B. Although B cells from ACB.*Col2*^{R360Q} mice express only a heavy chain knock-in and the C1 mutation is a single amino acid substitution rather than a complete deletion of the entire epitope, it was enough to limit the frequency and numbers of peripheral C1-B (Fig. 2, G–I). While it is true that the frequency and absolute number of C1-B remained unchanged in the BM of ACB.*Col2*^{R360Q} mice, light chain sequencing infers the presence of two main events that ensure the persistence of C1-B. The first one is "RAG-dependent VJ rearrangement" since V gene usage was found to be altered in B cells isolated from ACB and ACB.*Col2*^{R360Q}. The second event is dictated by activation-induced cytidine deaminase, an enzyme expressed by B cell precursors, which was shown to mediate B cell central tolerance (Kuraoka et al., 2011; Cantaert et al., 2015) and could also play a role in selecting autoreactive B cells since increased CDR3 mutations were found to be present in BM B cells isolated from ACB.*Col2*^{R360Q} mice without completely excluding the process of junctional diversity. Both events are associated with receptor editing, a mechanism that is initiated when BCR binds high-avidity autoantigens on immature B cells (Halverson et al., 2004). Based on the high avidity of COL2 due to the repetitive motifs formed by its fibrillar organization in cartilage in the BM and the relatively low affinity of C1-BCR, we propose that C1-B were selected even with the suboptimal 360Q C1 epitope on COL2 through changed V domains. In contrast to previously discovered CD5⁺ B-1 autoreactive cells (Hayakawa et al., 1999), our data clearly prove that a tissue-restricted self-antigen like COL2 can also positively select C1-specific conventional B2 cells defined by CD19 and B220 expression. It is likely that COL2 is one of a limited set of self-protein structures that select autoreactive B cells as a mechanism to maintain homeostasis in case inflammation occurs.

We also touch on the fine distinction that exists between poly- and mono-reactivity where a dominant expansion of triple helical polyreactive (GPO) over monoreactive (C1) B cells in RA embodies an imbalance that could result in an escalated B cell

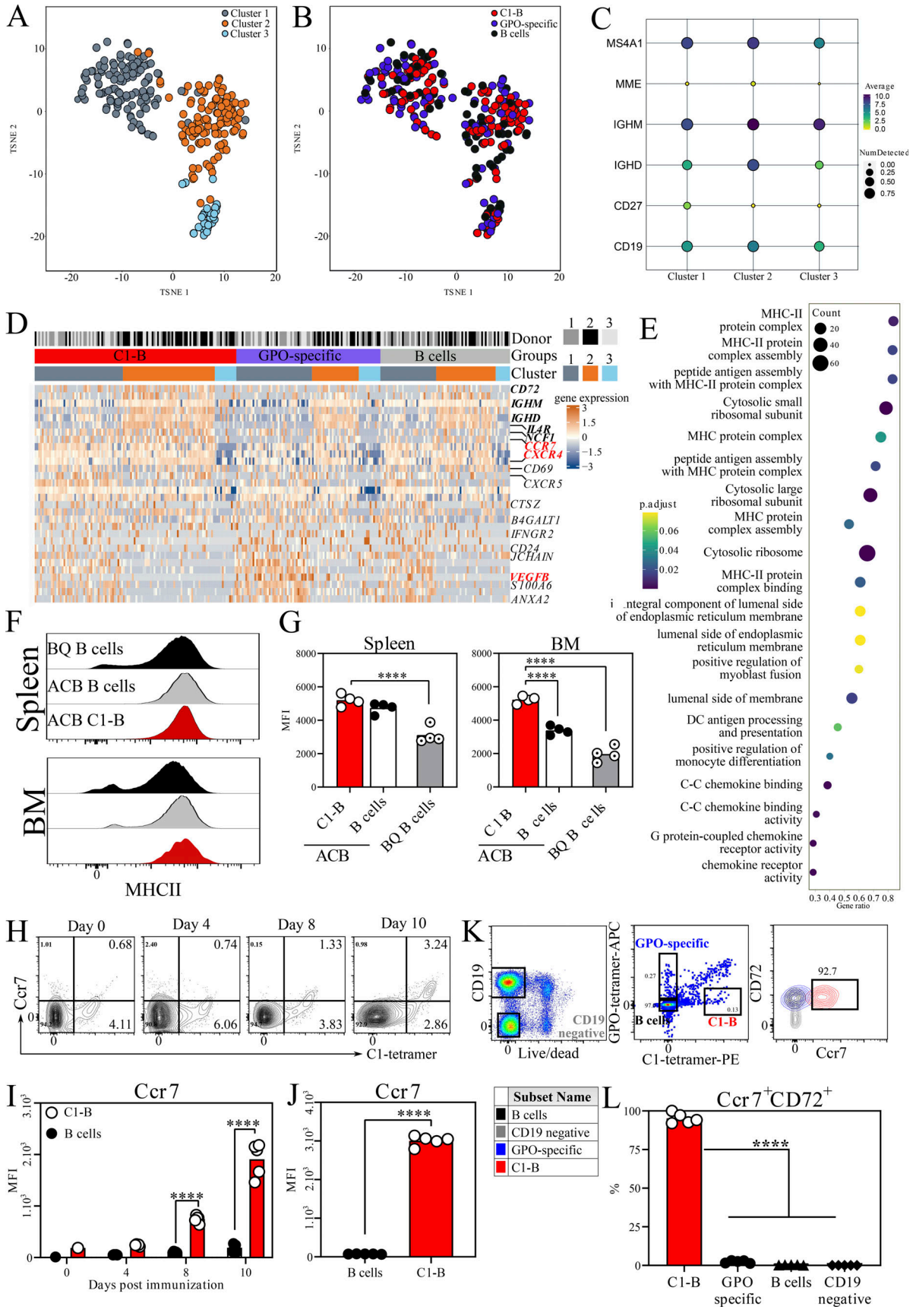

Figure 5. **Antigen-presenting C1-B upregulates CCR7 and CD72 upon activation. (A)** RNA sequencing of single sorted C1-B, GPO-specific, and B cells from HD (n = 3). Data presented as t-SNE. **(B)** The distribution of different groups within the clusters. **(C)** The expression of B cell subtype markers where a dot

represents each feature (row) in each group of cells (column). The proportion of detected expression values and the average expression for each feature in each group of cells is visualized using the size and color, respectively, of each dot. **(D)** Heatmap of selected immune-related genes that are significantly differentially expressed (in red) and belong to the top 50 differentially regulated genes but not statistically significant (in bold black). **(E)** The summary of top enriched terms between C1-B and GPO-specific B cells depicting the enrichment score, gene ratio, and gene count. **(F and G)** Representative flow cytometry plots and mean fluorescent intensity (MFI) quantification depicting surface MHCII expression on BM- and spleen-derived B cells from ACB and BQ mice (n = 4/group). **(H and I)** Frequency and MFI of CCR7 on circulating C1-B days after ACB immunization. **(J)** CCR7 MFI on natural C1-B derived from LN of 10 d immunized BQ mice. **(K and L)** LN from day 30 immunized BQ mice were stained ex vivo and analysis of CD72 and CCR7 was assessed on C1-B (red), GPO-specific (blue), B cells (black), and non-B cells (gray). Error bars represent mean ± SEM. Statistics in J were determined by two-tailed Mann–Whitney U test. Significance in I and L was determined by two-way ANOVA followed by Sidak's test. **P < 0.01 and ****P < 0.0001.

autoreactivity. This fits the notion that antibodies from mature human B cells exhibit high monoreactivity but low polyreactivity (Wardemann et al., 2003), while the reported increase in polyreactivity of mature naïve B cells from RA patients favors a defective B cell tolerance (Samuels et al., 2005). Our setup offers the possibility to identify molecular determinants that orchestrate the fate of natural autoreactive yet suppressive B cells. Also, these findings propose potential treatments that warrant thorough investigation. In particular, expanding C1-B cells has the potential to restore homeostasis and regulate arthritis.

The identification of an IL10-producing B cell subset that prevents the development of arthritis in the mouse did set the stage for the regulatory B cell field (Mauri et al., 2003). The terminology shifted to "B10" when IL10-competent B cells in mice and humans were found to also express CD1d and CD5 (Yanaba et al., 2008). Nonetheless, both B cell populations were hailed as important players in balancing autoimmune responses, a function primarily accomplished by the release of the anti-inflammatory IL10 cytokine (Dilillo et al., 2010). The antigen specificity of B10 has been hypothesized but has never been reported. The parallels that exist between C1-B and B10 cells, in terms of IL10 production and surface expression of CD1d/CD5, pushed us to ponder whether we unraveled the so-long anticipated antigen specificity of regulatory B cells. However, the independence of IL10 in suppressing arthritis and controlling T cell responses (Fig. 3, E–G and Fig. 4, I–K) placed C1-B distant to conventional B10 cells.

Our model also adds another functional layer that could motivate the need for antigen-specific autoreactive B cells. The escape of COL2-reactive T cells from intrathymic selection (Raposo et al., 2018) and their association with autoimmune arthritis (Bäcklund et al., 2002a, 2002b) begs this question: What peripheral mechanism governs antigen-specific tolerance? The COL2-specific T cell tolerance underlined by C1-B cells may provide the answer. B cells possess the ability to uptake and present specific antigens that other innate antigen-presenting cells non-specifically acquire exogenously by virtue of their BCR specificity (Lanzavecchia, 1990). After acquiring the antigen, B cells migrate to the T cell zone in the LN to engage with T cells in a CCR7-dependent manner (Okada et al., 2005). While the upregulation of CCR7 only after antigen sensitization on C1-B endorses these reports, the aftermath of the T–B interaction is often restricted to the antibody responses. Our data demonstrate that the outcome of this interaction favors the expansion of antigen-specific Tregs governed by CD72 on autoreactive B cells. The latest study deciphering the interactome diagram of the human immune system revealed that CD72 is majorly expressed in naïve B cells and binds to SEM4D protein with a relatively high binding strength (Shilts et al., 2022). Whether CD72-SEM4D contact activates or tolerizes T cells is subject to debate; however the noted decrease in C1-B coincides with the decrease in SEM4D expression on T cells and its association with disease activity in RA individuals (Yoshida et al., 2015; Ha et al., 2018). On the other hand, the complete lack of CD72 expression affects the development and activation of B cells (Pan et al., 1999) and an intact SEM4D-CD72 is vital for T cell proliferation (Jiang et al., 2017). Besides, CD72 is also gaining attention in the cancer field as its expression is enriched in different B cell malignancies, and incorporating CD72-specific nanobodies into the chimeric antigen receptors offers a promising cancer immunotherapeutic potential (Nix et al., 2021). Here, we showcase an unprecedented function for CD72 in expanding autoreactive Tregs which can have important clinical implications. For instance, coupling of SEM4D or CD72 agonist to a multimeric C1-construct may bind the C1-B BCR and the CD72 molecule simultaneously. This crosslinking can unleash the suppressive function of B cells enhancing their tolerization mechanism.

Autoantibodies continue to be a powerful diagnostic marker for various autoimmune diseases. Several groups were isolated, characterized, and proved the specificity of the somatically hypermutated autoantibodies against their cognate autoantigens (Mietzner et al., 2008; Guo et al., 2010). The unexpected high affinity to various autoantigens by the germline version of these autoantibodies in different autoimmune diseases was attributed to the impaired B cell tolerance checkpoints in patients (Harmer et al., 1995; Di Niro et al., 2012; Hargreaves et al., 2013; Fichtner et al., 2020). However, this notion fails to explain the observed autoreactivity in healthy individuals, suggesting that these autoantibodies may have originated from naïve autoreactive B cells (Cotzomi et al., 2019). Our model of tracing autoreactive B cells specific to a tissue protein allows a physiological selection of B cells against an antigen that is physiologically expressed in central (BM and thymus) and peripheral (cartilage, eye, and reproductive system according to the human protein atlas; Thul and Lindskog, 2018) tissues.

One limitation of our study is that we only investigated C1-B with enough affinity to bind the tetramer. It is possible that additional B cells were not identified due to their relatively low affinity to the tetramer, even in the heavy chain knock-in mice. The amino acid substitution ($COL2^{R360Q}$) mice highlighted this point as the efficiency of selection was clearly different between BM and LNs, possibly because the used amino acid substitution did not block all the epitope-specific B cells as it changed the affinity threshold for their interaction rather than prohibiting it.

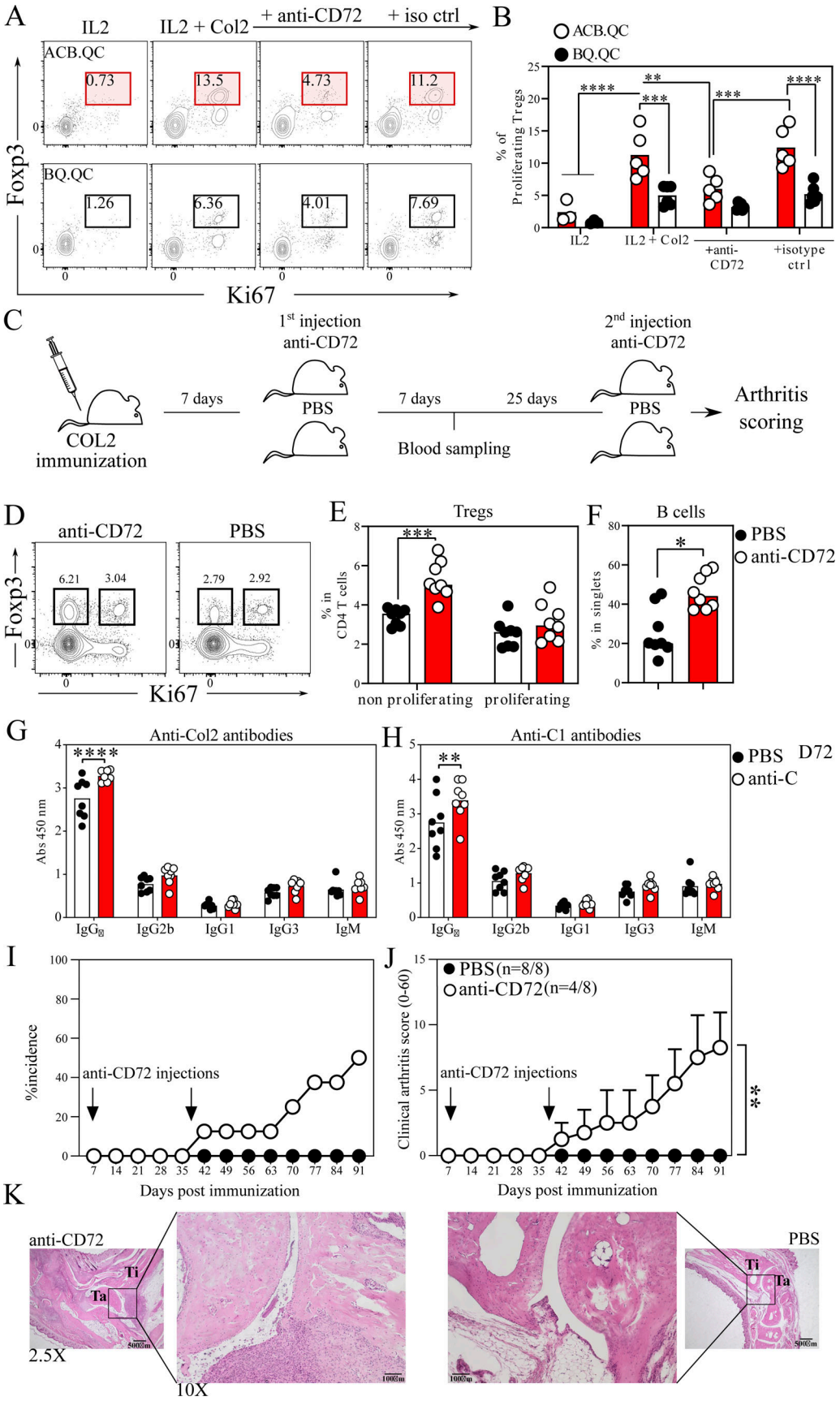

Figure 6. **Treg induction by C1-B is abrogated by blocking CD72. (A and B)** Flow cytometry plots depicting the proliferation of Tregs after culture of naïve LN in vitro from ACB.QC and BQ.QC mice in the presence of COL2 and mouse anti-mouse CD72 blocking antibody or mouse IgG1 isotype control. **(C)** Schematic

design of CD72 blocking in vivo. **(D and E)** Flow cytometry plots depicting the frequency of circulating proliferating (Ki67$^+$) and non-proliferating (Ki67$^-$) Foxp3$^+$ T cells in the blood (day 14 after COL2 immunization) of ACB mice injected anti-CD72 mAb or PBS (n = 8 mice/group). **(F)** Frequency of circulating B cells (CD19$^+$B220$^+$) cells as in D. **(G and H)** Serum titers of anti-COL2 and anti-C1 antibodies with different isotypes 14 d after immunization in anti-CD72 or PBS-treated groups. **(I and J)** Arthritis incidence and clinical score of CIA in ACB mice injected or not with anti-CD72 antibody. Only sick mice were plotted in J. **(K)** Representative histological H&E staining of tibia (Ti) and talus (Ta) in recipient mice. Error bars represent mean ± SEM. Statistics in E–H and J were determined by two-tailed Mann–Whitney U test. Significance in B was determined by two-way ANOVA followed by Sidak's test. *P < 0.05, **P < 0.01, ***P < 0.001, and ****P < 0.0001. Scale bar for 2.5× is 500 µm and for 10× is 100 µm.

Lastly, the growing interest in B cell–driven thymic selection and the ongoing debate about the origin of these B cells (Perera et al., 2013; Yamano et al., 2015), resident vs. migratory, make our system advantageous in this regard. Our in vitro and in vivo data show a strong antigen-specific Tregs expansion in direct contact with COL2-specific B cells, an event that besides peripheral lymphoid organs could even take place earlier, in the thymus, where triple helical COL2 is also expressed (Raposo et al., 2018). Analysis of thymic resident vs. migratory CCR7$^+$ COL2-specific B cell population may give in-depth evidence about their contribution to T cell selection and whether it is dictated by the autoimmune regulator (AIRE; Mathis and Benoist, 2009) expression.

It is likely, in similarity with the thymus, that certain epitopes exposed in central lymphoid organs lead to the clonal deletion of pathogenic lymphocytes whereas other epitopes select lymphocytes with regulatory functions. Although we have focused on one tissue-specific epitope, it is likely that there is a limited number of similar epitopes on proteins expressed in the BM and maybe also in other lymphoid organs, which selects an effective immune regulatory framework, in analogy with C1-B.

Materials and methods

Mice

All mice were on a B10Q background (short named BQ) and determined to be genetically identical using 10,000 single-nucleotide polymorphism typing, except for the targeted loci. Mice were screened using microsatellite markers surrounding the IgJH-targeted locus on chromosome 12. A mutation in the *Ncf1* gene (*m1J*; the coded protein also known as p47phox) in the BQ mice, designated as BQ.*Ncf1*$^{m1J/m1J}$ (abbreviated as BQ.*Ncf1*$^{*/*}$) impairs the expression of a functional NCF1 protein and thereby totally blocks the function of the NOX2 complexes, as previously described (Hultqvist et al., 2004; Sareila et al., 2013). BQ.*Ncf1*$^{*/*}$ mice were used as recipients for the transfer models in CIA and EAE. Tiger mice (IL10-GFP reporter mice) were purchased from Jackson Laboratory and were backcrossed to the ACB mice. IL10$^{-/-}$ mice were generated as previously described (Kühn et al., 1993) and were crossed to the ACB mice. COL2-specific T cell transgenic (Vα11.1 Vβ8.3) QC mice were used as a tool to study T cell responses (Brand et al., 2002). ACB.*Col2*^{R360Q} mice were generated by CRISPR/Cas9-guided point mutation at exon 25 (360 R to Q) of the *Col2a1* gene. All mice in this study were backcrossed to arthritis-permissive BQ^{rhd} mice expressing the MHCII allele A^q for more than 10 generations (Bäcklund et al., 2013). Anesthesia for animals was carried out by isoflurane inhalation and CO_2 was used for sacrifice. All experimental animal procedures were performed in accordance with local regulations and rules and were approved by "Stockholms djurförsöksetiska nämnd."

Animal experiments

Age-matched 8- to 12-wk-old male mice were used for experiments. All animals were kept in a climate-controlled environment in polystyrene cages (individually ventilated cages) containing wood shavings under specific pathogen–free conditions and with 12-h light/dark cycles. All experiments were blinded, with age- and sex-matched littermates randomly distributed in cages, following the ARRIVE standard. Animal welfare authorities (Stockholm region, Sweden) approved the animal experiments with permit numbers N35/16 and 2660-2021 for arthritis and N83/13 for EAE.

Patients and HD

Peripheral blood used in Fig. 1 and Fig. S1 was derived from patients with anti-citrullinated protein antibody–positive RA that were obtained at the outpatient clinic of the Division of Rheumatology at the Frankfurt University Hospital, Germany. All patients met the 2010 American College of Rheumatology/European League against Rheumatism criteria for RA at the time of diagnosis. Treatment regimens included conventional synthetic disease modifying antirheumatic drugs and glucocorticoids (<10 mg/d). Ethical approval was obtained by the committee of the University Hospital Frankfurt, Germany (reference number: 19/15). HD samples were acquired from Karolinska University Laboratory and the Deutsches Rotes Kreuz blood donation center in Frankfurt, Germany. No HD had developed clinical signs of arthritis and hence did not meet the 2010 American College of Rheumatology/European League against Rheumatism criteria for RA at the time of sampling. All donors gave informed consent. Permission for the conduct of the study was obtained from the ethical review board of Karolinska Institute.

Serum and cartilage samples

Serum samples, used in Fig. S1 F, from three different cohorts were employed. RA serum was derived from the TIRA-2 (2nd Early Intervention in RA) cohort (n = 504), which enrolled patients with recent-onset RA between 2006 and 2009 (Ziegelasch et al., 2020). Symptom duration was at least 6 wk but <12 mo. At the time of serum sampling (i.e., baseline), no patient was treated with conventional synthetic disease modifying antirheumatic drugs. Patients provided written and oral informed consent and ethical permission was granted (EPN-Linköping Dnr M168-05). In the BARFOT (Better Anti-Rheumatic PharmacOTherapy) cohort, a total of 621 patients with early untreated RA were included consecutively at the time of RA

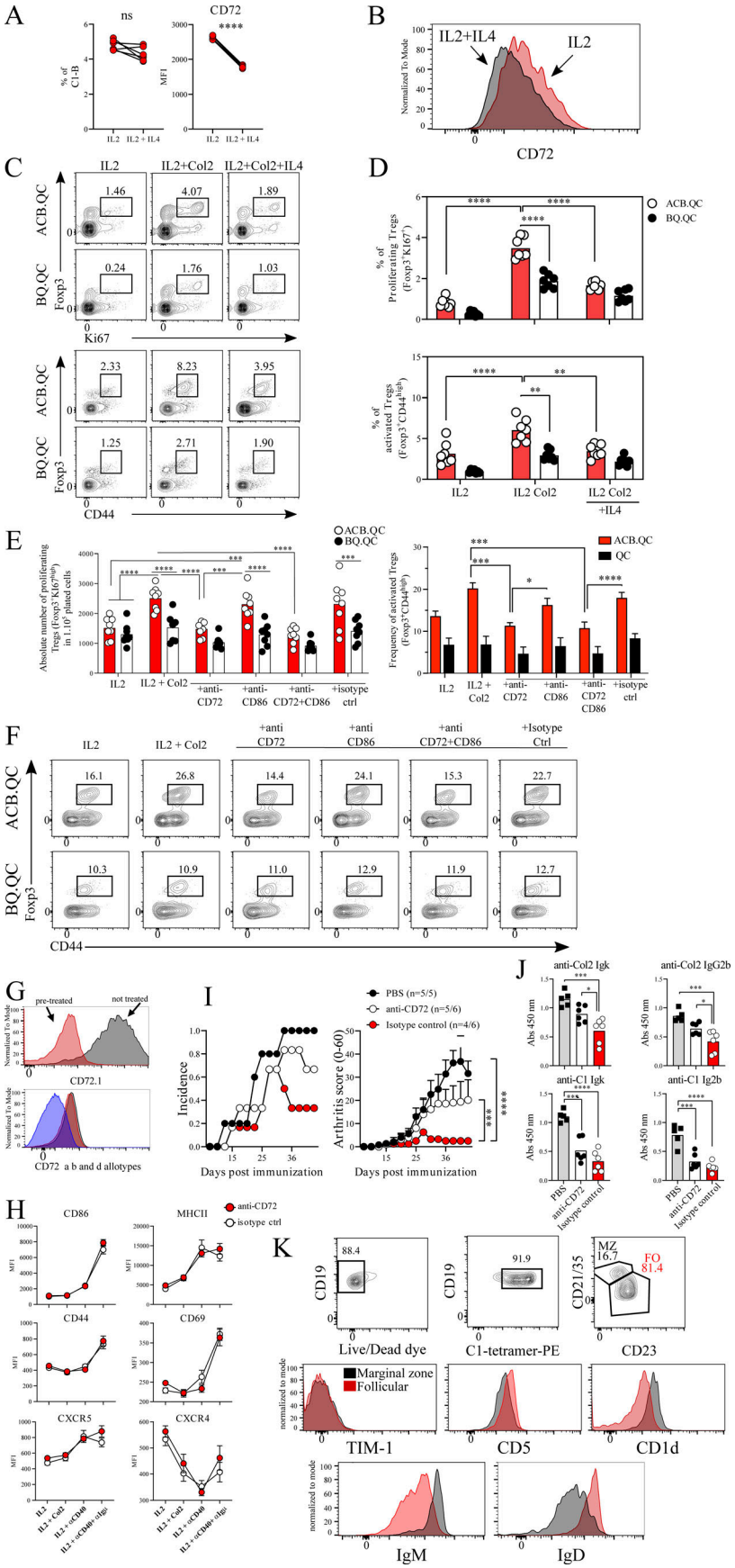

Figure 7. **CD72 controls Treg expansion and activation by C1-B. (A)** Frequency of C1-B and quantification of CD72 MFI on C1-B 24 h after the addition of IL4 to the culture. **(B)** Representative histograms exhibiting the expression of CD72 on C1-B from A. **(C)** Representative flow cytometry plot of the Foxp3$^+$Ki67$^+$ and Foxp3$^+$CD44^{high} gating 48 h after coculture of naïve iLN from ACB.QC and BQ.QC mice in the presence or absence of IL4. **(D)** Frequency of proliferating and activated Tregs from C. **(E)** Absolute number of proliferating Tregs and frequency of activated Tregs within the Vβ8.3$^+$CD4$^+$ population after blocking CD86. **(F)** Representative flow cytometry plot of the Foxp3$^+$CD44^{high} gating 48 h after coculture of naïve iLN from ACB.QC and BQ.QC mice in the presence or absence of different blocking antibodies. **(G)** Representative histogram validating the blockade of CD72. **(H)** MFI quantification of antigen presentation-related proteins (CD86, MHCII), activation markers (CD44, CD69), and chemokine receptors (CXCR5 and CXCR4) on 48 h cultured B cells after anti-CD72 or isotype control treatment in the presence of different stimuli. **(I)** Isolated C1-B were treated ex vivo with blocking CD72 antibody (anti-CD72) or isotype control following adoptive transfer into syngeneic BQ.*Ncf1*^{m1j} recipient mice. Arthritis incidence and clinical score in BQ.*Ncf1*^{m1j} recipient mice are plotted. **(J)** Titer of anti-COL2 and anti-C1 IgG antibody measured by ELISA in the sera of recipient mice 25 d after CIA. **(K)** Flow cytometry plots and histograms exhibiting the surface expression of certain markers on transferred C1-B in I. Error bars represent mean ± SEM. Statistical significance in A was determined using paired *t* test, while in D, E, I, and J, it was determined using one way ANOVA followed by Sidak's correction test. *P < 0.05, **P < 0.01, ***P < 0.001, and ****P < 0.0001.

diagnosis between 1999 and 2006, and ethical permission was approved by the Regional Ethical Review Board Lund and Stockholm, Sweden (Dnr 2016/297-31/1; Hafström et al., 2019). As controls, we used age- and gender-matched population controls without any known rheumatic diseases from the Malmö Diet and Cancer cohort (n = 398). The different clinical cohort studies were performed according to the Helsinki Declaration. All patients and the population controls signed informed consent and the study protocols were approved by regional ethics review boards.

Bead-based multiplex immunoassays

Antibody responses in human sera were analyzed by using the Luminex platform, as described previously (Tong et al., 2018). NeutrAvidin (Thermo Fischer Scientific) was coupled to magnetic carboxylated beads (Magplex Microspheres, Luminex Corp) after which biotinylated COL2 peptides were immobilized to the beads. Serum samples were diluted 1:100 (vol/vol) and purified antibodies were diluted into an assay buffer (3% BSA, 5% milk powder, 0.05% Tween 20, 100 µg/ml NeutrAvidin in PBS) and incubated for 1 h at room temperature (RT) on a shaker. The samples were then transferred to a 96-well plate (Greiner Bio-One) containing the peptide-coated beads. After incubation at RT on a shaker for 75 min, the beads were washed with 0.05% Tween-20 in PBS (PBST) on a plate washer (Bioplex Pro Wash station; Bio-Rad) and resuspended in a solution (PBST, 3% BSA) containing the secondary anti-human or anti-mouse IgG Fcγ-PE (#109-116-170; Jackson ImmunoResearch Laboratories). After 40 min of incubation, the beads were washed with PBST and the fluorescence intensity was measured using the Bio-plex 200 instrument (Bio-Rad).

Antigens and tetramer preparation

Rat COL2 was obtained from pepsin-digested SWARM chondrosarcoma and subsequently processed as previously described (Andersson and Holmdahl, 1990). C1 THP C1: (GPO)5-GDOGROGEOGLOGARGLTGROGDA-(GPO)5 and GPO control GPO: (GPO)11 were synthesized using a protocol previously reported (Viljanen et al., 2020). Both tetramers were prepared by mixing THP biotinylated peptides with streptavidin-R-PE/BV421/APC at a 4.5:1 ratio. Both tetramers were titrated down to 5–12 nM when used for staining and sorting procedures. T cell–specific epitopes (259–273) on rat COL2 with an unmodified lysine at position 264 (native) or with a galactose residue as a PTM on the same lysine were synthesized as previously described (Broddefalk et al., 1998).

Flow cytometry

All centrifugation steps were carried out at 300 g for 8 min at RT; 1 × 10^6 cells were blocked in 20 µl of PBS containing 5 µg in-house produced 2.4G2 in 96-well plates for 10 min at RT. Samples were washed with 150 µl of PBS and subsequently stained with the indicated antibodies in 20 µl of PBS diluted 1:100 or 1:200 at 4°C for 20 min in the dark (see antibody list). Cells were washed once, fixed, and permeabilized for intracellular staining using BD Cytofix/Cytoperm (BD) according to the manufacturer's instructions. Cells were stained intracellularly with 20 µl of permeabilization buffer (BD) and antibodies at a 1:100 final dilution for 20 min at RT. FoxP3 and Ki67 staining required nuclear permeabilization and was carried out using Bioscience Transcription Factor Staining Buffer.

Antibodies

The following reagents were purchased from BioLegend: anti-rat CD45 (OX-1), anti-rat CD45RA (OX-33), anti-rat CD4 (W3/25), anti-rat CD11b/c (OX-42), anti-CD21/CD35 (7e9), anti-CD24 (M169), anti-CD23 (B3B4), anti-IgD (11-26c.2a), anti-CD44 (IM7), anti-CD19 (6D5), anti-CD5 (53-7.5), anti-MHCII (2G9), anti-CD4 (H129.19), anti-CXCR4 (L276F12), anti-CXCR5 (L138D7), anti-CD86 (GL-1), anti-IL10 (JES5-16E3), anti-IL2 (JES6-5H4), anti-IL17 (TC1118H10.1), anti-IFNg (R46A2), anti-CCR7 (4B12), anti-human CD14 (HCD14), anti-human CD3 (OKT3). Reagents purchased from BD are as follows: anti-CD49b (DX5), anti-IgM (R6-60.2 and 11/41), anti-TIM-1 (RMT1-4), anti-CD1d (1B1), anti-CD93 (AA4.1), anti-CD4 (RM4-5), anti-CD3 (145-2C11), anti-CD25 (PC61), anti-B220 (RA3-6B2), anti-CD72 abd alloantigen (K10.6), anti-CD11b (M170), anti-human CD19 (SJ25C1). Reagents purchased from eBioscience are as follows: anti-Ki67 (SolA15), anti-TCRb (H57-597), anti-Foxp3 (FJK-16s), anti-rat CD45R (His24). Live/dead fixable dyes for discrimination of dead cells were purchased from Thermo Fisher Scientific, and three formats were used: green, near-infrared, and violet.

Magnetic bead–based enrichment

C1-B

Typically, five spleens were mashed and pooled, and single-cell suspensions were prepared from naïve or immunized animals. Cells were stained with C1-PE tetramer for 15 min at 4°C, washed twice, and incubated for 10 min with MACS anti-PE microbeads (100 µl of beads to 400 µl of MACS buffer). Cells were washed again and loaded onto LS columns and washed three times with 3 ml MACS buffer. C1-B were eluted by flushing 5 ml of MACS buffer using the plunger. Collected cells were counted, stained for surface markers, and analyzed by Attune NxT (Thermo Fisher Scientific) or LSR II (BD).

PE-B

The enrichment protocol for PE-specific B cells was done according to previously published method (Pape et al., 2011). Briefly, spleens were mashed, and single-cell suspensions were prepared from naïve or PE-immunized animals (50 µl/mouse intradermal emulsion consisting of 50 µg PE in CFA). Cells were stained with 1 µg PE (# P801; Invitrogen) for 30 min at 4°C, washed twice, and incubated for 15 min at 4°C with 50 µl MACS anti-PE microbeads. Cells were washed again, loaded onto LS columns, and washed three times with 3 ml MACS buffer. PE-B were eluted by flushing 5 ml of MACS buffer using the plunger. Collected cells were counted, stained for surface markers, and analyzed by Attune NxT (Thermo Fisher Scientific) or LSR II (BD).

C1-B sorting by fluorescence-activated cell sorting

Three to four spleens from naïve and immunized mice were pooled and single-cell suspensions were prepared for T cell and

myeloid cell depletion. Briefly, pelleted cells were stained with TCRβ and CD11b biotinylated antibodies and washed extensively after 15 min incubation at RT. Cells were suspended in MACS buffer and incubated with anti-biotin microbeads (#130-090-485; Miltenyi Biotec) for 15 min at 4°C followed by a washing step. Next, cells were passed through LD columns and washed two times with 1 ml MACS buffer. Collected unbound cells were resuspended in PBS and stained for CD19/B220, C1-tetramer, and live/dead dye to be further sorted via BD FACSAria III. Cells were gated for live, $CD19^+B220^+$ and sorted depending on C1-tetramer staining. 0.5 to 1 million pure (>90% purity) $C1^-$ B cells and $C1^+$ B cells were collected for downstream application. For human single-cell sorting, buffy coats from healthy blood donors were purchased from the transfusion unit at Karolinska Hospital (Solna, Stockholm), and PBMCs were isolated via density gradient centrifugation using Ficoll-Paque Plus (#17144002; Cytiva) in SepMate-50 (#85450; Stemcell Technologies) tubes. Cells were counted and stained with C1-PE tetramer for 15 min at RT. Next, cells were washed twice with MACS buffer and anti-PE beads were added for 10 min at 4°C followed by a washing step. Cells were passed through LS columns according to the manufacturer's protocol. Collected C1-B cells were stained with dead cells discriminator dye and anti-human antibodies, CD3, CD14, CD19, GPO-tetramer-APC. C1-tetramer$^+$ B cells (Live/$CD3^-CD14^-$/$CD19^+$/GPO-tetramer$^-$), GPO-tetramer$^+$ cells (Live/$CD3^-CD14^-$/$CD19^+$/C1-tetramer$^-$), and random B cells (Live/$CD3^-CD14^-$/$CD19^+$/GPO and C1-tetramer$^-$) and single-cell sorted into 96 or 384 well plates via BD FACSAria III.

CIA in recipient mice after adoptive transfer

Transfer experiments in Fig. 3, A and E were carried out using naïve ACB, ACB.*IL10*$^{-/-}$, BQ, and BQ.*IL10*$^{-/-}$ donor male mice that were sacrificed, and untouched B cells were isolated from spleens. A total of 5 × 10^6 B cells were adoptively transferred intravenously to syngeneic recipient male BQ.*Ncf1*^{m1j} 1 d prior to COL2 immunization. The transfer experiment in Fig. 3 H included a secondary step where C1-B enrichment was carried out after B cell isolation (purity; Fig. S3 G). 2–5 × 10^5 C1-B and naïve B cells were then adoptively transferred intravenously to syngeneic recipient male BQ.*Ncf1*^{m1j} 1 d prior to COL2 immunization.

8- to 12-wk-old male mice were immunized intradermally at the base of the tail with 100 µg of COL2 in 0.1 M acetic acid emulsified with an equal volume (1:1) of complete Freund's adjuvant (#263810; Nordic Biolabs) in a total volume of 100 µl. Clinical signs of CIA were assessed blindly three times per week using the scoring system based on the number of inflamed joints in each paw. Inflammation was defined by swelling and redness. One point was given to each inflamed toe or knuckle and five points to each inflamed wrist or ankle, resulting in a total possible score of 0–15 per paw and 0–60 per mouse.

For anti-CD72 treatment in Fig. 6 C, ACB mice were immunized at day 0 and a single 50 µg dose of unlabeled mouse anti-mouse CD72 (#1725-01; SouthernBiotech) was administered intravenously at day 7 and 39 after COL2 immunization.

For the adoptive experiment in Fig. 7 I, 12 × 10^6 C1-B were enriched and purified from ACB LNs and spleens and blocked ex vivo with either 100 µg anti-mouse CD72 or isotype control for 1 h. Approximately 1–2 × 10^6 C1-B were adoptively transferred intravenously to syngeneic recipient male BQ.*Ncf1*^{m1j} 1 d prior to COL2 immunization. A PBS group was added as a control for the transfer.

MOG-induced EAE

Mice were immunized with 100 µl of an emulsion containing 100 µg of MOG78-96 peptide or protein MOG1-125 in PBS and 50 µl of complete Freund's adjuvant (#263810; Nordic Biolabs). All animals were boosted with 200 ng of *Bordetella pertussis* toxin (#70323-44-3; Sigma Aldrich) in PBS intraperitoneally on day 0 and 48 h after immunization. From day 7 onwards, mice were scored for clinical manifestations as follows: 0, no clinical signs; 1, tail weakness; 2, tail paralysis; 3, tail paralysis and mild waddle; 4, tail paralysis and severe waddle; 5, tail paralysis and paralysis of one limb; 6, tail paralysis and paralysis of two limbs; 7, tetraparesis; and 8, moribund or deceased.

Histology

Histopathology

Hind paws were fixed in paraformaldehyde (4% wt/vol), decalcified in EDTA, and embedded in paraffin. Sections were stained with hematoxylin and eosin, and inflammation was scored on a 30-point scale. Points were attributed as follows: synovium hyperplasia (2), infiltration (2), angiogenesis (2), pannus formation (2), necrosis (2), cartilage erosion (2), bone erosion (2) or new formation (2), joint structure destruction (6), and ankylosis (6). Ankle joints from arthritic mice were taken at the end of CIA (typically day 90 after immunization).

Immunofluorescence

Neonatal and adult mice were injected with 100 µg of biotinylated CB20 antibody intravenously, and mice were sacrificed 24 h later. The femurs were immediately snap-frozen in optimal cutting temperature compound (prechilled with liquid nitrogen) and kept at −70°C until cryosectioned. Staining was carried out as described earlier (Li et al., 2020) and sections were visualized using Carl Zeiss LSM800 confocal microscope. Image processing and Zen software.

Determination of anti-COL2 antibody response by enzyme-linked immunosorbent assay

During the CIA disease course, blood samples from experimental mice were collected through the cheek bleeding technique on different days. All serum samples were used for analysis of the COL2-specific antibody response by enzyme-linked immunosorbent assay (ELISA). Nunc MaxiSorp ELISA plates (#423501; BioLegend) were coated with either rat COL2 or the synthetic COL2 fragments at 4°C, incubated overnight, and blocked with 1% bovine serum albumin in PBS for 1 h at RT. Mouse sera were titrated in PBS-T and loaded on the plates for 1 h at RT. Antibody binding was detected either by using horseradish peroxidase (HRP)–conjugated goat anti-mouse total IgG (#115-035-062; Jackson Immuno Research Laboratories), bio-anti kappa (produced in-house, clone 187.1), or biotin-conjugated secondary antibodies for immunoglobulin subclass/isotype-specific ELISA. Streptavidin-HRP (#117K4758; Sigma-Aldrich) was added to the

bioconjugated secondary antibodies, and 2,2-azino-di-(3-ethylbenzthiazoline sulfonate) diammonium salt (2,2′-azino-bis(acido 3-etilbenzotiazolina-6-solfonico) tablets, #11204521001; Sigma-Aldrich) or 3,3′,5,5′ tetramethylbenzidine (TMB; #S-100-TMB; Seramun Diagnostica) were used as substrates. The absorbance value was measured at 405 or 450 nm, respectively.

Assay for COL2 presentation by B cells

Spleen cells prepared from ACB and BQ mice were separated by magnetic sorting using anti-B220 microbeads as described by the manufacturer (#130-049-501; Miltenyi Biotec). The purity of the $B220^+$ cells was measured by flow cytometry. In the cell culture, 5×10^4 specific T cell hybridoma cells (HCQ3; Raposo et al., 2018) were cocultured with 5×10^5 purified B cells and antigen (COL2) in a total volume of 200 µl in U-bottom 96-well plates. We titrated the antigens while the amount of T cell hybridomas and B cells were kept constant. After 24 h culturing time at 37°C, supernatants were removed and IL2 levels were measured by ELISA. As negative controls, we used T cell hybridomas incubated with B cells without antigen, T cell hybridomas incubated with antigen without B cells, and T cell hybridoma culture in the medium without any other cells. The values for IL2 content are depicted as random fluorescence units, detected by europium-labeled streptavidin using the dissociation-enhanced lanthanide fluoroimmunoassay (#1244-360; DELFIA) system. In some assays, MACS-purified ACB B cells were prefixed with 0.5% paraformaldehyde for 15 min at RT and then washed three times with PBS before use in COL2 presentation assays. For in vivo pulsing of B cells, ACB and BQ mice were injected intravenously with COL2 or ovalbumin (100 µg/mouse). Mice were sacrificed 24 h later and spleen cells were MACS purified for B cell isolation. Purified B cells were used in COL2 presentation assays without adding any exogenous antigen.

For the experiment in Fig. 4 and Fig. S4 B cells from the BQ, ACB and ACB.$Col2^{360Q}$ mice were isolated from naïve spleens using a B cell isolation untouched mouse kit (#130-090-862; Miltenyi). In Fig. 4 I, C1-B enrichment was used after B cell isolation. Next, primary COL2-specific transgenic T cells were isolated from naïve QC mice using the CD4 T cell isolation untouched Dynabeads kit (#11415D; Thermo Fisher Scientific). 0.5×10^6 B cells were co-cultured with 0.5×10^6 T cells for 48 h at 37°C 5% CO_2 in the presence or absence of COL2 peptides at 20 ug/ml and IL2 (#212-12; Peprotech) at 3.3 ng/ml. After that, cells were washed with PBS and analyzed in the flow cytometry.

For the experiment in Fig. 6 (A and B) and Fig. 7 (E and F), 1×10^6 and 1×10^5, respectively, naïve LN cells derived from ACB.QC and BQ.QC mice were cultured in vitro in the presence or absence of IL2, COL2, anti-CD72 (10.1.D2), anti-CD86 (GL-1), both, or IgG2b/IgG2a isotype controls for 48 h at 37°C 5% CO_2. After that, cells were washed with PBS and analyzed in the flow cytometry.

For the experiment in Fig. 7 (C and D), 1×10^6 naïve LN cells derived from ACB.QC and BQ.QC mice were cultured in vitro in the presence or absence of IL2, COL2, and IL4 (Peprotech) at 2 ng/ml for 48 h at 37°C 5% CO_2. After that, cells were washed with PBS and analyzed in the flow cytometry.

scRNA-seq and analysis

Human buffy coats from three donors were magnetically enriched for C1-B and then single cells were sorted in a 384-well plate. Cell lysis, RNA denaturation, reverse transcription, PCR pre-amplification, and library preparation was carried out according to the Smart-seq3 protocol (Hagemann-Jensen et al., 2020). Raw counts were demultiplexed and summarized using zUMIs (Holland et al., 2020). Counts summarized to exons were analyzed using Scater (McCarthy et al., 2017) and Scran (Lun et al., 2016); Wilcoxon sum rank test was used for detecting differentially expressed genes.

Functional annotation was performed by Gene Set Enrichment Analysis (Subramanian et al., 2005) using Clusterprofiler (Yu et al., 2012) with gene sets from Gene Ontology (Ashburner et al., 2000) and Reactome (Griss et al., 2020). Plots illustrating functional annotation analysis were generated using the Enrichplot package and heatmaps were generated using ComplexHeatmap package.

Ex vivo expansion of human B cells

Complete B cell medium was prepared using RPMI (Gibco) supplemented with 10% ultra-low IgG fetal bovine serum (#FCS.ULIgG.0500; Bio&Sell), 1× MEM non-essential amino acids (#11140-050; GIBCO), 1 mM sodium pyruvate (#11360-070; GIBCO), 50 µM β-mercaptoethanol (#31350-010; GIBCO), and penicillin/streptomycin (#P4333; Sigma-Aldrich). We supplemented the complete medium with 10 ng/ml recombinant human IL21 (Peprotech), 50 ng/ml recombinant human IL2 (Peprotech), 30 µg/ml human holo-transferrin (#616424; Merck Millipore), and 2.5 µg/ml ODN 2006 (5′-TCGTCGTTTTGTCGTTTTGTCGTT-3′ with a nuclease-resistant phosphorothioate backbone; # HC4039; Hycult Biotech). C1 B cells were enriched magnetically from HD PBMC and single-cell sorted into tissue culture–treated 96-well U-bottom plates (#353077; Falcon) prefilled with 1×10^4 CD40L-expressing irradiated fibroblasts (50 Gy dose) in 200 µl of complete B cell medium per well. Cells were cultured for a period of 2 wk at 37°C in humidified air with 5% CO_2. Culture supernatants were carefully aspirated and screened for anti-C1, anti-GPO, total IgG, and IgM antibodies.

Immunoglobulin cloning

The molecular cloning protocol was carried out as previously described (Lindner et al., 2019) with minor modifications. The expanded B cells in the cell culture plates were lysed with 30 µl/well lysis buffer (100 mM Tris-HCl pH 7.5, 500 mM lithium chloride, 10 mM EDTA pH 8.0, 5 mM dithiothreitol, 1% wt/vol lithium dodecyl sulfate). Plates were quickly frozen on dry ice and stored at −80°C until further use. The 96-well plates containing the B cell lysates were thawed and selected lysates aspirated and transferred to a 96-well plate prefilled with oligo-dT coated magnetic beads (Dynabeads Oligo(dT) by #61002; Invitrogen) for mRNA extraction. The mRNA was extracted according to the manufacturer's instructions, followed by on-bead reverse transcription to cDNA using Ig-specific oligonucleotide primers and SuperScript IV reverse transcriptase (#4311235; Thermo Fisher Scientific). The cDNA was then subjected to three separate PCR rounds amplifying variable heavy (VH), variable

kappa (Vκ), and variable lambda (Vλ) gene segments using a multiplexed set of forward primers to bind Ig variable regions and two reverse primers binding in the constant heavy 1 (CH1) region of IGHG and IGHM, respectively. PCRs were performed with Phusion High-Fidelity DNA polymerase (#F530L; Thermo Fisher Scientific) using primer sets described by Lindner et al. (2019).

PCR products were purified using Mag-Bind RxnPure Plus magnetic beads (#M1386-00; Omega Bio-Tek). After purification, heavy/kappa/lambda PCR products were subjected to sequencing using respective reverse primers. After sequencing, selected PCR products were amplified and restriction NotI/XhoI restriction sites were introduced by nested PCR using a multiplexed forward primer set annealing to FR1 and a multiplexed reverse primer set annealing to FR4/J segment of the VH/Vκ/Vλ sequence.

The amplified PCR product was purified, digested, and cloned into a pcDNA3.4 backbone plasmid containing the hIGHG1 heavy constant and hIGKC kappa constant sequence, respectively. The ligation was transformed into Library Efficiency DH5α Competent cells (#18263012; Thermo Fisher Scientific) and cultured overnight on LB-Agar + carbenicillin plates. For each cloning sample, four clones were placed into 96-well deep well plates (VWR #732–2892) prefilled with 1 ml LB, sealed, and cultured overnight at 37°C with 800 rpm shaking.

For plasmid isolation, 96-well filter plates were used (#8175; Pall) together with buffers from the QIAGEN Plasmid Maxi kit (#12165). The protocol follows the typical plasmid purification steps: alkaline lysis, neutralization, filtration, and isopropanol precipitation of plasmid DNA. This procedure ensures transfection-grade plasmid quality. Subsequently, the plasmid sequence was confirmed by Sanger sequencing using cytomegalovirus forward sequencing primer.

Plasmids with correct in-frame sequence were cotransfected (heavy + light) into 3 ml transfection-ready Expi293F suspension cells in six-well cell culture plates using FectoPRO (Polyplus transfection) according to the manufacturer's instructions. The cells were cultured at 37°C, 130 rpm, 80% humidity for 5 d. IgG was purified from the supernatant using Protein G GraviTrap columns according to the manufacturer's instructions.

The recombinant antibodies were tested against their original antigen targets using ELISA. ELISA plates (#442404; Thermo Fisher Scientific) were coated with 5 µg/ml streptavidin in PBS, followed by the addition of 1 µg/ml biotinylated C1 THP in PBS for 30 min at RT. Plates were washed once with PBST and recombinant antibody was added at 5 µg/ml in PBS + 0.5% BSA for 2 h at RT. Plates were washed three times with PBST and secondary HRP goat anti-human IgG (#2040-05; Southern Biotech) was added at 1 µg/ml for 1 h at RT, after which plates were again washed three times with PBST. 50 µl of TMB substrate (#S-100-TMB; Seramun Diagnostica) was added and incubated until signal saturation; 0.3 M sulfuric acid was added to stop the reaction. A450 was measured using a Synergy Reader (BioTek).

Antibody sequence analysis

Immunoglobulin heavy and light chain sequences were analyzed using IgBLAST (Ye et al., 2013) with the IMGT database as a reference (Lefranc et al., 2015).

Proteomic sample preparation

$C1^+$ (bound to C1-tetramer) and $C1^-$ B (unbound fraction) cells from ACB mice were pelleted and lysed in 50 mM Tris buffer pH 7.5 containing 8 M urea, 1% SDS, and protease inhibitor (cOmplete Protease Inhibitor; Roche). Samples were sonicated and proteins were reduced with 5 mM dithiothreitol at RT for 1 h followed by alkylation using 15 mM iodoacetamide at RT in the dark for 1 h. Chloroform/methanol precipitation of protein was performed as follows: three volumes (compared with sample) of methanol were added, followed by one volume of chloroform and three volumes of water. Then samples were vortexed and centrifuged for 10 min at 20,000 *g* at 4°C. The aqueous phase was carefully removed and the protein pellet was washed with one volume of methanol, vortexed, and centrifuged again. The liquid was removed, and the protein pellet was air-dried. Air-dried pellets were resuspended in 50 mM HEPES pH 8.5 containing 8 M urea. Urea concentration was diluted to 4 M and proteins were digested overnight with LysC (1:100 wt/wt), followed by trypsin (1:100 wt/wt) digestion for 6 h in 1 M urea. Tandem mass tag labeling was performed with a fourfold excess of labels compared with protein (wt/wt) in a final acetonitrile concentration of 20% for 2 h. The remaining labels were quenched with 0.5% triethylamine for 15 min, and samples were pooled and dried in a speed-vac until about 50% of the sample volume was evaporated. Samples were then acidified using trifluoroacetic acid (pH < 3) and desalted using Sep Pack (Waters). Cleaned samples were dried in a speed-vac and stored at −80°C.

Offline high pH reverse-phase fractionation for the first and second experiment was performed with an Ultimate 3000 RSLCanon System (Dionex) or an EASY-nLC 1000 system (Thermo Fisher Scientific Scientific), respectively, and concatenated into 12 fractions (Sabatier et al., 2018; Perez-Riverol et al., 2019). Mass spectra were acquired using parameters listed in Table 2.

Bioinformatics and data analysis for proteomics

Raw files were processed by an in-house modified version of MaxQuant software (version 1.6.2.3) recognizing TMTpro. For peptide search, acetylation of N-terminal, oxidation of methionine, and deamidation of asparagine and glutamine were selected as variable modifications, whereas carbamidomethylation of the cysteine was selected as a fixed modification. Trypsin with up to two missed cleavages was set as protease and the spectrum was searched against the UniProt mus musculus database (55,220 entries). The false discovery rate was set to 0.01 for both peptides and proteins. For all other parameters, the default settings were used.

All downstream analyses of proteomics data were done in R (R project). Known contaminants, decoy proteins, or proteins identified by site as well as proteins with fewer than two peptides were excluded from further analysis. Protein intensities were normalized by VSN and statistical differences between groups were calculated by a *t* test with equal or unequal variance depending on the F-test.

Statistics

All statistical analyses were performed using GraphPad Prism and R software. Statistical significance and error bars are indicated in figure legends.

Table 2. **LC-MS/MS parameters**

LC system	Ultimate 3000
Gradient	5 min (4% buffer B), 80 min (26%), 5 min (32%), 5 min (95%), 5 min (95%), 1 min (4%), 9 min (4%)
Mass spectrometer	Fusion lumos
Scan cycle	3 s
MS1 resolution	120,000
MS1 scan range	400–1,600 daltons
Injection time	50 s
AGC for MS1	10^6
APD	On
Included charge states	2–6
Exclusion duration	60 s
Isolation windows	1.6 dalton
NCE	35%
MS2 resolution	60,000
Injection time	Dynamic
AGC for MS2	125,000

LC-MS/MS, liquid chromatography–tandem mass spectrometry; APD, advanced peak determination; NCE, normalized collision energy; AGC, automatic gain control.

Online supplemental material

Fig. S1 shows the gating in different species and the displayed reduction of C1-B frequency in RA patients. Fig. S2 shows the altered V gene usage and somatic hypermutation of BM-derived C1-B in ACB.*Col2*^{R360Q} mice. Fig. S3 highlights the suppressive function of C1-B and their ability to produce IL-10. Fig. S4 demonstrates the capability of C1-B to activate Tregs in vitro, while Fig. S5 validates the expression of CCR7 and CD72 in naïve autoreactive C1-B.

Data availability

The mass spectrometry proteomics data files have been deposited to the ProteomeXchange Consortium (http://proteomecentral.proteomexchange.org) via the PRIDE partner repository (Perez-Riverol et al., 2019) with the data identifier PXD025837. The raw sequencing data presented in Fig. 5 (A–E) contains sensitive information that cannot be shared openly. However, processed data has been deposited at ArrayExpress and can be accessed with the identifier E-MTAB-13291.

Acknowledgments

We thank the Eukaryotic Single Cell Genomics facility at SciLifeLab for single-cell RNA sequencing. We thank Agata Smialowska from the National Bioinformatics Infrastructure Sweden for the bioinformatics support. The computations were performed on resources provided by the Swedish National Infrastructure for Computing through the Uppsala Multidisciplinary Center for Advanced Computational Science (UPPMAX) under project sens2021588. We thank Maria Lindskog for kindly sharing inbred rats. We thank Juan Basile and the Biomedicum Flow Cytometry Core Facility for their technical assistance. We thank Emma Mondoc from the Biomedicum Histological Core Facility for histology support and Kristina and Carlos Palestro for the exquisite animal handling.

This project was supported by Knut och Alice Wallenbergs Stiftelse (to R. Holmdahl; 2019.0059), Vetenskapsrådet (to R. Holmdahl; 2019-01209), Stiftelsen Konung Gustaf V:s 80-årsfond and Karolinska Institutet Foundation Grants for Rheumatology Research 2021 (to M. Aoun; SGI-2022-0862 and 2022-02852, respectively), HORIZON EUROPE Marie Sklodowska-Curie Actions (to A. Coelho and A. Krämer; 765158), Bundesministerium für Bildung und Forschung (to H. Burkhardt; project 4 01 EC 1009C). The funders had no role in study design, data collection and analysis, decision to publish, or preparation of the manuscript.

Author contributions: M. Aoun, A. Saxena, and R. Holmdahl designed the research; M. Aoun, A. Coelho, and A. Saxena performed most of the experiments, including acquiring and analyzing data. A. Krämer and B. Xu contributed to the cloning and expression of anti-C1 mAbs. P. Sabatier, C.M. Beusch, and R.A. Zubarev performed and analyzed the proteomic studies. Z. Xu and L. Romero Castillo performed the intravenous injections. N.N. Do and H. Burkhardt provided experimental data on RA-derived cells. N.N. Do, H. Burkhardt, C. Sjöwall, A. Kastbom, and I. Gjertsson contributed samples from human cohorts including human cartilage samples. J. Viljanen and J. Kihlberg produced and analyzed the peptides used for tetramers; Y. He, G. Fernandez Lahore, and E. Lönnblom performed the Luminex assays. H. Abolhassani analyzed light chain sequencing data. R. Holmdahl conceptualized the research, revised the manuscript, supervised, and took the overall responsibility for the study. All authors revised and approved the manuscript.

Disclosures: E. Lönnblom reported “other” from Vacara AB outside the submitted work. H. Burkhardt reported grants from the Fraunhofer Cluster of Excellence Immune-Mediated Diseases during the conduct of the study. R. Holmdahl is a founder of a biotech company, Vacara AB, but it is not directly related to this work. He also has consultancy fees from two small companies, Lipum AB and Cyxone AB, but these engagements are not related. No other disclosures were reported.

Submitted: 16 January 2023
Revised: 31 May 2023
Accepted: 16 August 2023

References

Andersson, M., and R. Holmdahl. 1990. Analysis of type II collagen-reactive T cells in the mouse. I. Different regulation of autoreactive vs. non-autoreactive anti-type II collagen T cells in the DBA/1 mouse. *Eur. J. Immunol.* 20:1061–1066. https://doi.org/10.1002/eji.1830200517

Bäcklund, J., A. Treschow, R. Bockermann, B. Holm, L. Holm, S. Issazadeh-Navikas, J. Kihlberg, and R. Holmdahl. 2002a. Glycosylation of type II collagen is of major importance for T cell tolerance and pathology in collagen-induced arthritis. *Eur. J. Immunol.* 32:3776–3784. https://doi.org/10.1002/1521-4141(200212)32:12<3776::AID-IMMU3776>3.0.CO;2-A

Bäcklund, J., S. Carlsen, T. Höger, B. Holm, L. Fugger, J. Kihlberg, H. Burkhardt, and R. Holmdahl. 2002b. Predominant selection of T cells specific for the glycosylated collagen type II epitope (263-270) in humanized transgenic mice and in rheumatoid arthritis. *Proc. Natl. Acad. Sci. USA*. 99:9960–9965. https://doi.org/10.1073/pnas.132254199

Bäcklund, J., C. Li, E. Jansson, S. Carlsen, P. Merky, K.S. Nandakumar, S. Haag, J. Ytterberg, R.A. Zubarev, and R. Holmdahl. 2013. C57BL/6 mice need MHC class II Aq to develop collagen-induced arthritis dependent on autoreactive T cells. *Ann. Rheum. Dis.* 72:1225–1232. https://doi.org/10.1136/annrheumdis-2012-202055

Brand, D.D., L.K. Myers, K.B. Whittington, K.A. Latham, J.M. Stuart, A.H. Kang, and E.F. Rosloniec. 2002. Detection of early changes in autoimmune T cell phenotype and function following intravenous administration of type II collagen in a TCR-transgenic model. *J. Immunol.* 168: 490–498. https://doi.org/10.4049/jimmunol.168.1.490

Broddefalk, J., J. Bäcklund, F. Almqvist, M. Johansson, R. Holmdahl, and J. Kihlberg. 1998. T cells recognize a glycopeptide derived from type II collagen in a model for rheumatoid arthritis. *J. Am. Chem. Soc.* 120: 7676–7683. https://doi.org/10.1021/ja980489k

Burkhardt, H., T. Koller, A. Engström, K.S. Nandakumar, J. Turnay, H.G. Kraetsch, J.R. Kalden, and R. Holmdahl. 2002. Epitope-specific recognition of type II collagen by rheumatoid arthritis antibodies is shared with recognition by antibodies that are arthritogenic in collagen-induced arthritis in the mouse. *Arthritis Rheum.* 46:2339–2348. https://doi.org/10.1002/art.10472

Cancro, M.P. 2020. Age-associated B cells. *Annu. Rev. Immunol.* 38:315–340. https://doi.org/10.1146/annurev-immunol-092419-031130

Cantaert, T., J.N. Schickel, J.M. Bannock, Y.S. Ng, C. Massad, T. Oe, R. Wu, A. Lavoie, J.E. Walter, L.D. Notarangelo, et al. 2015. Activation-induced cytidine deaminase expression in human B cell precursors is essential for central B cell tolerance. *Immunity*. 43:884–895. https://doi.org/10.1016/j.immuni.2015.10.002

Cao, D., Ia. Khmaladze, H. Jia, E. Bajtner, K.S. Nandakumar, T. Blom, J.A. Mo, and R. Holmdahl. 2011. Pathogenic autoreactive B cells are not negatively selected toward matrix protein collagen II. *J. Immunol.* 187: 4451–4458. https://doi.org/10.4049/jimmunol.1101378

Chen, J.W., J.N. Schickel, N. Tsakiris, J. Sng, F. Arbogast, D. Bouis, D. Parisi, R. Gera, J.M. Boeckers, F.R. Delmotte, et al. 2022. Positive and negative selection shape the human naive B cell repertoire. *J. Clin. Invest.* 132: e150985. https://doi.org/10.1172/JCI150985

Ashburner, M., C.A. Ball, J.A. Blake, D. Botstein, H. Butler, J.M. Cherry, A.P. Davis, K. Dolinski, S.S. Dwight, J.T. Eppig, et al. 2000. Gene ontology: Tool for the unification of biology. The gene ontology consortium. *Nat. Genet.* 25:25–29. https://doi.org/10.1038/75556

Cotzomi, E., P. Stathopoulos, C.S. Lee, A.M. Ritchie, J.N. Soltys, F.R. Delmotte, T. Oe, J. Sng, R. Jiang, A.K. Ma, et al. 2019. Early B cell tolerance defects in neuromyelitis optica favour anti-AQP4 autoantibody production. *Brain*. 142:1598–1615. https://doi.org/10.1093/brain/awz106

Csomos, K., B.Ujhazi, P.Blazso, J.L.Herrera, C.M.Tipton, T.Kawai, S.Gordon, M.Ellison, K.Wu, M.Stowell, et al. 2022. Partial RAG deficiency in humans induces dysregulated peripheral lymphocyte development and humoral tolerance defect with accumulation of T-bet$^+$ B cells. *Nat. Immunol.* 23:1256–1272. https://doi.org/10.1038/s41590-022-01271-6

Di Niro, R., L.Mesin, N.Y.Zheng, J.Stamnaes, M.Morrissey, J.H.Lee, M.Huang, R.Iversen, M.F.du Pré, S.W.Qiao, et al. 2012. High abundance of plasma cells secreting transglutaminase 2-specific IgA autoantibodies with limited somatic hypermutation in celiac disease intestinal lesions. *Nat. Med.* 18:441–445. https://doi.org/10.1038/nm.2656

Dilillo, D.J., T. Matsushita, and T.F. Tedder. 2010. B10 cells and regulatory B cells balance immune responses during inflammation, autoimmunity, and cancer. *Ann. N Y Acad. Sci.* 1183:38–57. https://doi.org/10.1111/j.1749-6632.2009.05137.x

Fichtner, M.L., C. Vieni, R.L. Redler, L. Kolich, R. Jiang, K. Takata, P. Stathopoulos, P.A. Suarez, R.J. Nowak, S.J. Burden, et al. 2020. Affinity maturation is required for pathogenic monovalent IgG4 autoantibody development in myasthenia gravis. *J. Exp. Med.* 217:e20200513. https://doi.org/10.1084/jem.20200513

Fidler, A.L., S.P. Boudko, A. Rokas, and B.G. Hudson. 2018. The triple helix of collagens - an ancient protein structure that enabled animal multicellularity and tissue evolution. *J. Cell Sci.* 131:jcs203950. https://doi.org/10.1242/jcs.203950

Gagliani, N., C.F. Magnani, S. Huber, M.E. Gianolini, M. Pala, P. Licona-Limon, B. Guo, D.R. Herbert, A. Bulfone, F. Trentini, et al. 2013. Coexpression of CD49b and LAG-3 identifies human and mouse T regulatory type 1 cells. *Nat. Med.* 19:739–746. https://doi.org/10.1038/nm.3179

Goodnow, C.C., J. Crosbie, S. Adelstein, T.B. Lavoie, S.J. Smith-Gill, R.A. Brink, H. Pritchard-Briscoe, J.S. Wotherspoon, R.H. Loblay, K. Raphael, et al. 1988. Altered immunoglobulin expression and functional silencing of self-reactive B lymphocytes in transgenic mice. *Nature*. 334:676–682. https://doi.org/10.1038/334676a0

Gottardi, R., U. Hansen, R. Raiteri, M. Loparic, M. Düggelin, D. Mathys, N.F. Friederich, P. Bruckner, and M. Stolz. 2016. Supramolecular organization of collagen fibrils in healthy and osteoarthritic human knee and hip joint cartilage. *PLoS One*. 11:e0163552. https://doi.org/10.1371/journal.pone.0163552

Griss, J., G. Viteri, K. Sidiropoulos, V. Nguyen, A. Fabregat, and H. Hermjakob. 2020. ReactomeGSA - efficient multi-omics comparative pathway analysis. *Mol. Cell. Proteomics*. 19:2115–2125. https://doi.org/10.1074/mcp.TIR120.002155

Guo, W., D. Smith, K. Aviszus, T. Detanico, R.A. Heiser, and L.J. Wysocki. 2010. Somatic hypermutation as a generator of antinuclear antibodies in a murine model of systemic autoimmunity. *J. Exp. Med.* 207: 2225–2237. https://doi.org/10.1084/jem.20092712

Ha, Y.J., D.W. Han, J.H. Kim, S.W. Chung, E.H. Kang, Y.W. Song, and Y.J. Lee. 2018. Circulating semaphorin 4D as a marker for predicting radiographic progression in patients with rheumatoid arthritis. *Dis. Markers*. 2018:2318386. https://doi.org/10.1155/2018/2318386

Hafström, I., S. Ajeganova, M.L. Andersson, S.V. Bala, S. Bergman, A. Bremander, K. Forslind, K. Malm, and B. Svensson. 2019. A Swedish register-based, long-term inception cohort study of patients with rheumatoid arthritis—results of clinical relevance. *Open Access Rheumatol.* 11:207–217. https://doi.org/10.2147/OARRR.S218448

Hagemann-Jensen, M., C. Ziegenhain, P. Chen, D. Ramsköld, G.J. Hendriks, A.J.M. Larsson, O.R. Faridani, and R. Sandberg. 2020. Single-cell RNA counting at allele and isoform resolution using Smart-seq3. *Nat. Biotechnol.* 38:708–714. https://doi.org/10.1038/s41587-020-0497-0

Halverson, R., R.M. Torres, and R. Pelanda. 2004. Receptor editing is the main mechanism of B cell tolerance toward membrane antigens. *Nat. Immunol.* 5:645–650. https://doi.org/10.1038/ni1076

Hargreaves, C.E., M. Grasso, C.S. Hampe, A. Stenkova, S. Atkinson, G.W. Joshua, B.W. Wren, A.M. Buckle, D. Dunn-Walters, and J.P. Banga. 2013. Yersinia enterocolitica provides the link between thyroid-stimulating antibodies and their germline counterparts in Graves' disease. *J. Immunol.* 190:5373–5381. https://doi.org/10.4049/jimmunol.1203412

Harmer, I.J., S. Loizou, K.M. Thompson, A.K. So, M.J. Walport, and C. Mackworth-Young. 1995. A human monoclonal antiphospholipid antibody that is representative of serum antibodies and is germline encoded. *Arthritis Rheum.* 38:1068–1076. https://doi.org/10.1002/art.1780380808

Hayakawa, K., M. Asano, S.A. Shinton, M. Gui, D. Allman, C.L. Stewart, J. Silver, and R.R. Hardy. 1999. Positive selection of natural autoreactive B cells. *Science*. 285:113–116. https://doi.org/10.1126/science.285.5424.113

Holland, C.H., J. Tanevski, J. Perales-Patón, J. Gleixner, M.P. Kumar, E. Mereu, B.A. Joughin, O. Stegle, D.A. Lauffenburger, H. Heyn, et al. 2020. Robustness and applicability of transcription factor and pathway analysis tools on single-cell RNA-seq data. *Genome Biol.* 21:36. https://doi.org/10.1186/s13059-020-1949-z

Holmdahl, R., K. Rubin, L. Klareskog, E. Larsson, and H. Wigzell. 1986. Characterization of the antibody response in mice with type II collagen-induced arthritis, using monoclonal anti-type II collagen antibodies. *Arthritis Rheum.* 29:400–410. https://doi.org/10.1002/art.1780290314

Holmdahl, R., M. Andersson, T.J. Goldschmidt, K. Gustafsson, L. Jansson, and J.A. Mo. 1990. Type II collagen autoimmunity in animals and provocations leading to arthritis. *Immunol. Rev.* 118:193–232. https://doi.org/10.1111/j.1600-065X.1990.tb00817.x

Hu, H., B. Wang, M. Borde, J. Nardone, S. Maika, L. Allred, P.W. Tucker, and A. Rao. 2006. Foxp1 is an essential transcriptional regulator of B cell development. *Nat. Immunol.* 7:819–826. https://doi.org/10.1038/ni1358

Hultqvist, M., P. Olofsson, J. Holmberg, B.T. Bäckström, J. Tordsson, and R. Holmdahl. 2004. Enhanced autoimmunity, arthritis, and encephalomyelitis in mice with a reduced oxidative burst due to a mutation in the Ncf1 gene. *Proc. Natl. Acad. Sci. USA*. 101:12646–12651. https://doi.org/10.1073/pnas.0403831101

Jiang, X., N.K. Björkström, and E. Melum. 2017. Intact CD100-CD72 interaction necessary for TCR-induced T cell proliferation. *Front. Immunol.* 8: 765. https://doi.org/10.3389/fimmu.2017.00765

Karlsson, R., J.A. Mo, and R. Holmdahl. 1995. Binding of autoreactive mouse anti-type II collagen antibodies derived from the primary and the secondary immune response investigated with the biosensor technique.

J. Immunol. Methods. 188:63–71. https://doi.org/10.1016/0022-1759(95)00203-0

Khmaladze, Ia., A. Saxena, K.S. Nandakumar, and R. Holmdahl. 2015. B-cell epitope spreading and inflammation in a mouse model of arthritis is associated with a deficiency in reactive oxygen species production. *Eur. J. Immunol.* 45:2243–2251. https://doi.org/10.1002/eji.201545518

Kühn, R., J. Löhler, D. Rennick, K. Rajewsky, and W. Müller. 1993. Interleukin-10-deficient mice develop chronic enterocolitis. *Cell*. 75:263–274. https://doi.org/10.1016/0092-8674(93)80068-P

Kuraoka, M., T.M. Holl, D. Liao, M. Womble, D.W. Cain, A.E. Reynolds, and G. Kelsoe. 2011. Activation-induced cytidine deaminase mediates central tolerance in B cells. *Proc. Natl. Acad. Sci. USA*. 108:11560–11565. https://doi.org/10.1073/pnas.1102571108

Lanzavecchia, A. 1990. Receptor-mediated antigen uptake and its effect on antigen presentation to class II-restricted T lymphocytes. *Annu. Rev. Immunol.* 8:773–793. https://doi.org/10.1146/annurev.iy.08.040190.004013

Lefranc, M.P., V. Giudicelli, P. Duroux, J. Jabado-Michaloud, G. Folch, S. Aouinti, E. Carillon, H. Duvergey, A. Houles, T. Paysan-Lafosse, et al. 2015. IMGT®, the international ImMunoGeneTics information system® 25 years on. *Nucleic Acids Res.* 43:D413–D422. https://doi.org/10.1093/nar/gku1056

Li, Y., D. Tong, P. Liang, E. Lönnblom, J. Viljanen, B. Xu, K.S. Nandakumar, and R. Holmdahl. 2020. Cartilage-binding antibodies initiate joint inflammation and promote chronic erosive arthritis. *Arthritis Res. Ther.* 22:120. https://doi.org/10.1186/s13075-020-02169-0

Lindner, J.M., V. Cornacchione, A. Sathe, C. Be, H. Srinivas, E. Riquet, X.C. Leber, A. Hein, M.B. Wrobel, M. Scharenberg, et al. 2019. Human memory B cells harbor diverse cross-neutralizing antibodies against BK and JC polyomaviruses. *Immun. Elsevier Inc.* 50:668–676.e5. https://doi.org/10.1016/j.immuni.2019.02.003

Lun, A.T.L., D.J. Mccarthy, and J.C. Marioni. 2016. A step-by-step workflow for low-level analysis of single-cell RNA-seq data with bioconductor. *F1000 Res.* 5:2122. https://doi.org/10.12688/f1000research.9501.2

Mathis, D., and C. Benoist. 2009. Aire. *Annu. Rev. Immunol.* 27:287–312. https://doi.org/10.1146/annurev.immunol.25.022106.141532

Mauri, C., D. Gray, N. Mushtaq, and M. Londei. 2003. Prevention of arthritis by interleukin 10-producing B cells. *J. Exp. Med.* 197:489–501. https://doi.org/10.1084/jem.20021293

McCarthy, D.J., K.R. Campbell, A.T. Lun, and Q.F. Wills. 2017. Scater: Pre-processing, quality control, normalization and visualization of single-cell RNA-seq data in R. *Bioinformatics*. 33:1179–1186. https://doi.org/10.1093/bioinformatics/btw777

Mietzner, B., M. Tsuiji, J. Scheid, K. Velinzon, T. Tiller, K. Abraham, J.B. Gonzalez, V. Pascual, D. Stichweh, H. Wardemann, and M.C. Nussenzweig. 2008. Autoreactive IgG memory antibodies in patients with systemic lupus erythematosus arise from nonreactive and polyreactive precursors. *Proc. Natl. Acad. Sci. USA*. 105:9727–9732. https://doi.org/10.1073/pnas.0803644105

Mo, J.A., C.A. Bona, and R. Holmdahl. 1993. Variable region gene selection of immunoglobulin G-expressing B cells with specificity for a defined epitope on type II collagen. *Eur. J. Immunol.* 23:2503–2510. https://doi.org/10.1002/eji.1830231019

Mo, J.A., A. Scheynius, S. Nilsson, and R. Holmdahl. 1994. Germline-encoded IgG antibodies bind mouse cartilage in vivo: Epitope- and idiotype-specific binding and inhibition. *Scand. J. Immunol.* 39:122–130. https://doi.org/10.1111/j.1365-3083.1994.tb03350.x

Nandakumar, K.S., L. Svensson, and R. Holmdahl. 2003. Collagen type II-specific monoclonal antibody-induced arthritis in mice: Description of the disease and the influence of age, sex, and genes. *Am. J. Pathol.* 163:1827–1837. https://doi.org/10.1016/S0002-9440(10)63542-0

Nemazee, D.A., and K. Bürki. 1989. Clonal deletion of B lymphocytes in a transgenic mouse bearing anti-MHC class I antibody genes. *Nature*. 337:562–566. https://doi.org/10.1038/337562a0

Nix, M.A., K. Mandal, H. Geng, N. Paranjape, Y.T. Lin, J.M. Rivera, M. Marcoulis, K.L. White, J.D. Whitman, S.P. Bapat, et al. 2021. Surface proteomics reveals cd72 as a target for in vitro–evolved nanobody-based car-t cells in kmt2a/mll1-rearranged b-all. *Cancer Discov.* 11:2032–2049. https://doi.org/10.1158/2159-8290.CD-20-0242

Ohl, L., M. Mohaupt, N. Czeloth, G. Hintzen, Z. Kiafard, J. Zwirner, T. Blankenstein, G. Henning, and R. Förster. 2004. CCR7 governs skin dendritic cell migration under inflammatory and steady-state conditions. *Immunity*. 21:279–288. https://doi.org/10.1016/j.immuni.2004.06.014

Okada, T., M.J. Miller, I. Parker, M.F. Krummel, M. Neighbors, S.B. Hartley, A. O'Garra, M.D. Cahalan, and J.G. Cyster. 2005. Antigen-engaged B cells undergo chemotaxis toward the T zone and form motile conjugates with helper T cells. *PLoS Biol.* 3:e150. https://doi.org/10.1371/journal.pbio.0030150

Olsson, L.M., Å.C. Johansson, B. Gullstrand, A. Jönsen, S. Saevarsdottir, L. Rönnblom, D. Leonard, J. Wetterö, C. Sjöwall, E. Svenungsson, et al. 2017. A single nucleotide polymorphism in the NCF1 gene leading to reduced oxidative burst is associated with systemic lupus erythematosus. *Ann. Rheum. Dis.* 76:1607–1613. https://doi.org/10.1136/annrheumdis-2017-211287

O'Neill, S.K., Y. Cao, K.M. Hamel, P.D. Doodes, G. Hutas, and A. Finnegan. 2007. Expression of CD80/86 on B cells is essential for autoreactive T cell activation and the development of arthritis. *J. Immunol.* 179:5109–5116. https://doi.org/10.4049/jimmunol.179.8.5109

Pan, C., N. Baumgarth, and J.R. Parnes. 1999. CD72-deficient mice reveal nonredundant roles of CD72 in B cell development and activation. *Immunity*. 11:495–506. https://doi.org/10.1016/S1074-7613(00)80124-7

Pape, K.A., J.J. Taylor, R.W. Maul, P.J. Gearhart, and M.K. Jenkins. 2011. Different B cell populations mediate early and late memory during an endogenous immune response. *Science*. 331:1203–1207. https://doi.org/10.1126/science.1201730

Perera, J., L. Meng, F. Meng, and H. Huang. 2013. Autoreactive thymic B cells are efficient antigen-presenting cells of cognate self-antigens for T cell negative selection. *Proc. Natl. Acad. Sci. USA*. 110:17011–17016. https://doi.org/10.1073/pnas.1313001110

Perez-Riverol, Y., A. Csordas, J. Bai, M. Bernal-Llinares, S. Hewapathirana, D.J. Kundu, A. Inuganti, J. Griss, G. Mayer, M. Eisenacher, et al. 2019. The PRIDE database and related tools and resources in 2019: Improving support for quantification data. *Nucleic Acids Res.* 47:D442–D450. https://doi.org/10.1093/nar/gky1106

Raposo, B., P. Merky, C. Lundqvist, H. Yamada, V. Urbonaviciute, C. Niaudet, J. Viljanen, J. Kihlberg, B. Kyewski, O. Ekwall, et al. 2018. T cells specific for post-translational modifications escape intrathymic tolerance induction. *Nat. Commun.* 9:353. https://doi.org/10.1038/s41467-017-02763-y

Rudge, E.U., A.J. Cutler, N.R. Pritchard, and K.G. Smith. 2002. Interleukin 4 reduces expression of inhibitory receptors on B cells and abolishes CD22 and Fc γ RII-mediated B cell suppression. *J. Exp. Med.* 195:1079–1085. https://doi.org/10.1084/jem.20011435

Sabatier, P., A.A. Saei, S. Wang, and R.A. Zubarev. 2018. Dynamic proteomics reveals high plasticity of cellular proteome: Growth-related and drug-induced changes in cancer cells are comparable. *Proteomics*. 18:e1800118. https://doi.org/10.1002/pmic.201800118

Samuels, J., Y.S. Ng, C. Coupillaud, D. Paget, and E. Meffre. 2005. Impaired early B cell tolerance in patients with rheumatoid arthritis. *J. Exp. Med.* 201:1659–1667. https://doi.org/10.1084/jem.20042321

Sareila, O., N. Jaakkola, P. Olofsson, T. Kelkka, and R. Holmdahl. 2013. Identification of a region in p47phox/NCF1 crucial for phagocytic NADPH oxidase (NOX2) activation. *J. Leukoc. Biol.* 93:427–435. https://doi.org/10.1189/jlb.1211588

Shankar, S., J. Stolp, S.C. Juvet, J. Beckett, P.S. Macklin, F. Issa, J. Hester, and K.J. Wood. 2022. Ex vivo-expanded human CD19^{+}TIM-1^{+} regulatory B cells suppress immune responses in vivo and are dependent upon the TIM-1/STAT3 axis. *Nat. Commun.* 13:3121. https://doi.org/10.1038/s41467-022-30613-z

Shilts, J., Y. Severin, F. Galaway, N. Müller-Sienerth, Z.S. Chong, S. Pritchard, S. Teichmann, R. Vento-Tormo, B. Snijder, and G.J. Wright. 2022. A physical wiring diagram for the human immune system. *Nature*. 608:397–404. https://doi.org/10.1038/s41586-022-05028-x

Subramanian, A., P. Tamayo, V.K. Mootha, S. Mukherjee, B.L. Ebert, M.A. Gillette, A. Paulovich, S.L. Pomeroy, T.R. Golub, E.S. Lander, and J.P. Mesirov. 2005. Gene set enrichment analysis: A knowledge-based approach for interpreting genome-wide expression profiles. *Proc. Natl. Acad. Sci. USA*. 102:15545–15550. https://doi.org/10.1073/pnas.0506580102

Taylor, J.J., R.J. Martinez, P.J. Titcombe, L.O. Barsness, S.R. Thomas, N. Zhang, S.D. Katzman, M.K. Jenkins, and D.L. Mueller. 2012. Deletion and anergy of polyclonal B cells specific for ubiquitous membrane-bound self-antigen. *J. Exp. Med.* 209:2065–2077. https://doi.org/10.1084/jem.20112272

Tedder, T.F. 2015. B10 cells: A functionally defined regulatory B cell subset. *J. Immunol.* 194:1395–1401. https://doi.org/10.4049/jimmunol.1401329

Thul, P.J., and C. Lindskog. 2018. The human protein atlas: A spatial map of the human proteome. *Protein Sci.* 27:233–244. https://doi.org/10.1002/pro.3307

Tong, D., E. Lönnblom, A.C.Y. Yau, K.S. Nandakumar, B. Liang, C. Ge, J. Viljanen, L. Li, M. Bâlan, L. Klareskog, et al. 2018. A shared epitope of collagen type XI and type II is recognized by pathogenic antibodies in mice and humans with arthritis. *Front. Immunol.* 9:451. https://doi.org/10.3389/fimmu.2018.00451

Uysal, H., R. Bockermann, K.S. Nandakumar, B. Sehnert, E. Bajtner, A. Engström, G. Serre, H. Burkhardt, M.M. Thunnissen, and R. Holmdahl. 2009. Structure and pathogenicity of antibodies specific for citrullinated collagen type II in experimental arthritis. *J. Exp. Med.* 206:449–462. https://doi.org/10.1084/jem.20081862

Viljanen, J., E. Lönnblom, C. Ge, J. Yang, L. Cheng, S. Aldi, W. Cai, A. Kastbom, C. Sjöwall, I. Gjertsson, et al. 2020. Synthesis of an array of triple-helical peptides from type II collagen for multiplex analysis of autoantibodies in rheumatoid arthritis. *ACS Chem. Biol.* 15:2605–2615. https://doi.org/10.1021/acschembio.0c00680

Wardemann, H., S. Yurasov, A. Schaefer, J.W. Young, E. Meffre, and M.C. Nussenzweig. 2003. Predominant autoantibody production by early human B cell precursors. *Science.* 301:1374–1377. https://doi.org/10.1126/science.1086907

Yamano, T., J. Nedjic, M. Hinterberger, M. Steinert, S. Koser, S. Pinto, N. Gerdes, E. Lutgens, N. Ishimaru, M. Busslinger, et al. 2015. Thymic B cells are licensed to present self antigens for central T cell tolerance induction. *Immun. Elsevier Inc.* 42:1048–1061. https://doi.org/10.1016/j.immuni.2015.05.013

Yanaba, K., J.D. Bouaziz, K.M. Haas, J.C. Poe, M. Fujimoto, and T.F. Tedder. 2008. A regulatory B cell subset with a unique CD1dhiCD5+ phenotype controls T cell-dependent inflammatory responses. *Immunity.* 28:639–650. https://doi.org/10.1016/j.immuni.2008.03.017

Ye, J., N.Ma, T.L.Madden, and J.M.Ostell. 2013. IgBLAST: An immunoglobulin variable domain sequence analysis tool. *Nucleic Acids Res.* 41:W34–W40. https://doi.org/10.1093/nar/gkt382

Yoshida, Y., A. Ogata, S. Kang, K. Ebina, K. Shi, S. Nojima, T. Kimura, D. Ito, K. Morimoto, M. Nishide, et al. 2015. Semaphorin 4D contributes to rheumatoid arthritis by inducing inflammatory cytokine production: Pathogenic and therapeutic implications. *Arthritis Rheumatol.* 67:1481–1490. https://doi.org/10.1002/art.39086

Yu, G., L.G. Wang, Y. Han, and Q.Y. He. 2012. clusterProfiler: An R package for comparing biological themes among gene clusters. *OMICS.* 16:284–287. https://doi.org/10.1089/omi.2011.0118

Zhao, J., J. Ma, Y. Deng, J.A. Kelly, K. Kim, S.Y. Bang, H.S. Lee, Q.Z. Li, E.K. Wakeland, R. Qiu, et al. 2017. A missense variant in NCF1 is associated with susceptibility to multiple autoimmune diseases. *Nat. Genet.* 49:433–437. https://doi.org/10.1038/ng.3782

Ziegelasch, M., A. Boman, K. Martinsson, I. Thyberg, C. Jacobs, B.M. Nyhäll-Wåhlin, A. Svärd, E. Berglin, S. Rantapää-Dahlqvist, T. Skogh, and A. Kastbom. 2020. Anti-cyclic citrullinated peptide antibodies are associated with radiographic damage but not disease activity in early rheumatoid arthritis diagnosed in 2006-2011. *Scand. J. Rheumatol.* 49:434–442. https://doi.org/10.1080/03009742.2020.1771761

Zikherman, J., R. Parameswaran, and A. Weiss. 2012. Endogenous antigen tunes the responsiveness of naive B cells but not T cells. *Nature.* 489:160–164. https://doi.org/10.1038/nature11311

JEM

Supplemental material

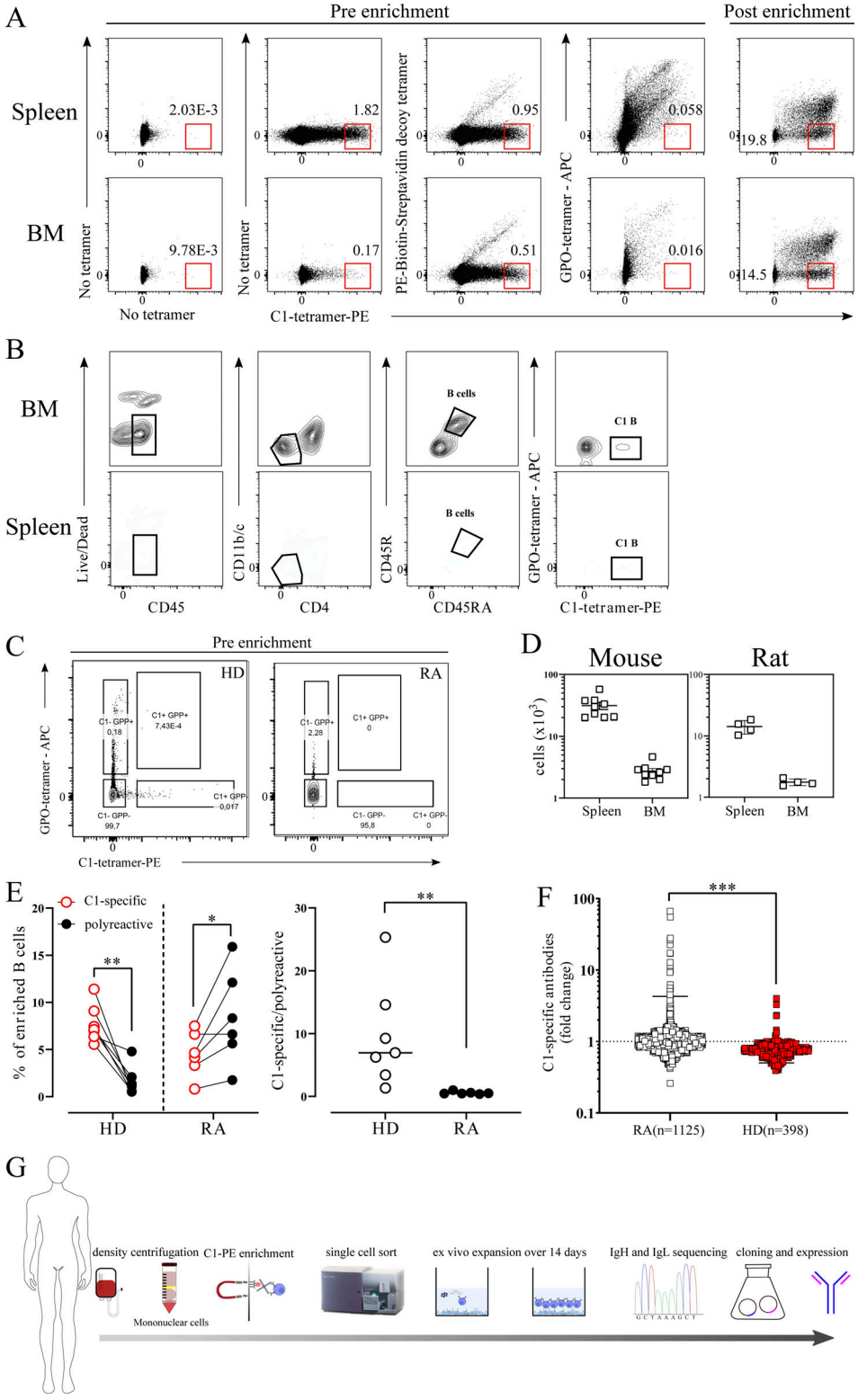

Figure S1. **C1-B frequency is reduced in RA patients. (A)** Representative flow cytometry staining of spleen and BM of BQ mice before and after enrichment in the absence of tetramers or in the presence of different control tetramers. **(B)** Representative flow cytometry staining of rat spleen and BM after C1-tetramer enrichment. **(C)** Representative flow cytometry staining of HD and RA PBMC before enrichment using C1- and GPO- tetramers. **(D)** The absolute number of C1-B in spleen and BM of mouse and rats. Each square represents one mouse or rat. **(E)** Frequency of C1-B and polyreactive (GPO) B cells in HD (n = 7) and RA patients (n = 6); each dot represents one donor. The ratio between C1-B and polyreactive B cells in HD and RA patients. **(F)** Luminex analysis of triple helical C1-specific antibody response in RA patients (n = 1,125) and age-matched HD (n = 398). **(G)** Schematic of the experimental design adopted to clone and express MAK antibodies. Error bars represent mean ± SEM. Statistical significance in E (% of enriched) was determined using a paired t test, while the ratio in F was determined using two-tailed Mann–Whitney U test. *P < 0.05, **P < 0.01, and ***P < 0.001.

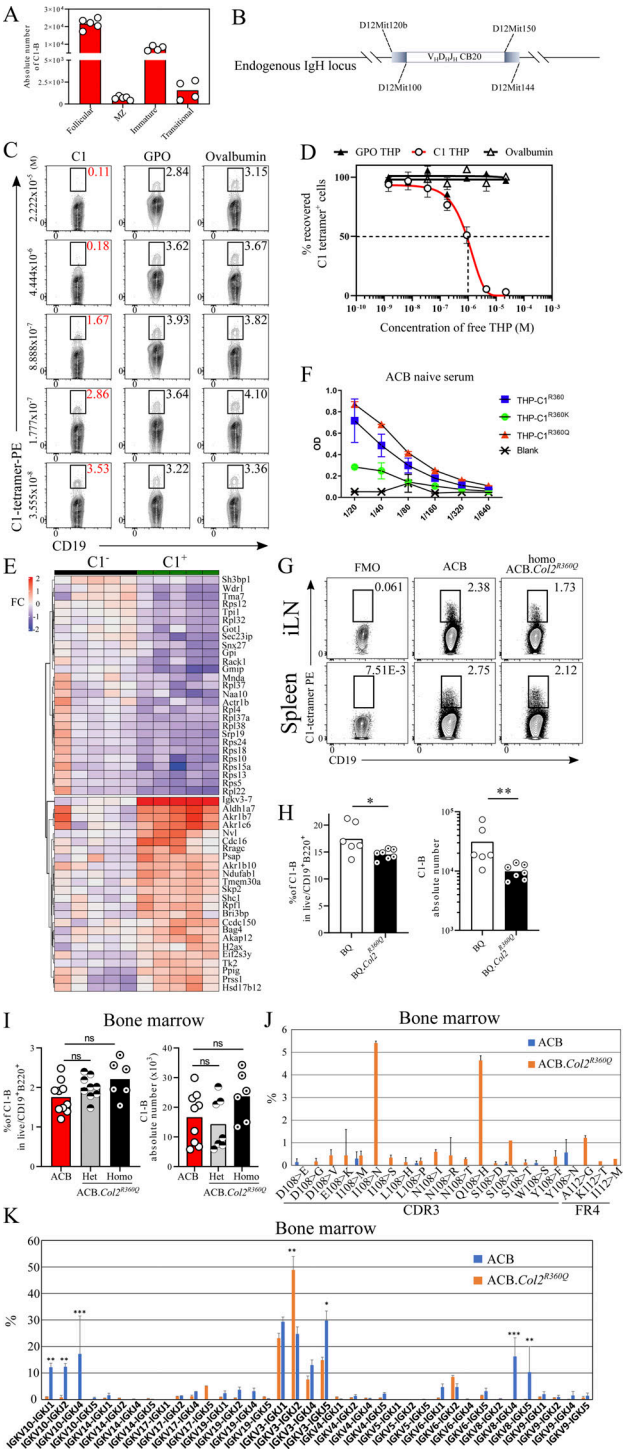

Figure S2. **Col2^{R360Q} mutation induces somatic hypermutation and alters the usage of the light chain by C1-B. (A)** Enumeration of C1-B at different stages of B cell development in BQ mice. Each dot represents one mouse. **(B)** Schematic representation of the CB20 VDJ knock-in ACB mouse. **(C)** Measuring median affinity of C1-B. Cells from the spleen and BM of ACB mice were split equally in sever wells and incubated with noted concentration (M) of C1 or GPO THP or ovalbumin protein before C1-tetramer staining and flow cytometric analysis. Representative flow cytometry plots showing the retrieval of C1-B after incubations. **(D)** Percent of recovered C1-B (C1-tetramer$^+$ B cells) is shown compared with the number of C1-B detected in the absence of competitor antigen. **(E)** Heatmap of significantly downregulated and upregulated proteins between C1$^+$ and C1$^-$ B cells. **(F)** Sera from naïve ACB at increasing dilutions tested for specificity against different THPs. **(G)** Representative flow cytometry plots exhibiting the frequency of C1-B detected in the spleen and inguinal LN (iLN) of ACB and ACB.*Col2*^{R360Q} mice. FMO controls were included for the C1-tetramer staining. **(H)** Frequency and absolute number of C1-B detected after C1 enrichment in the spleens of BQ and BQ.*Col2*^{R360Q} mice. Each dot represents one mouse. **(I)** Frequency and absolute number of C1-B detected in the BM of ACB and ACB.*Col2*^{R360Q} (het and homo). **(J)** Frequency of mutations in the CDR3 and FR4 light chain of enriched C1-B from BM of ACB and ACB.*Col2*^{R360Q} mice (n = 3/group). **(K)** V_k gene usage detected from light chain next-generation sequencing of enriched C1-B from ACB and ACB.*Col2*^{R360Q} (n = 3/group). Error bars represent mean ± SEM. Statistical significance in H–K was determined using two-tailed Mann–Whitney U test. *P < 0.05, **P < 0.01, and ***P < 0.001.

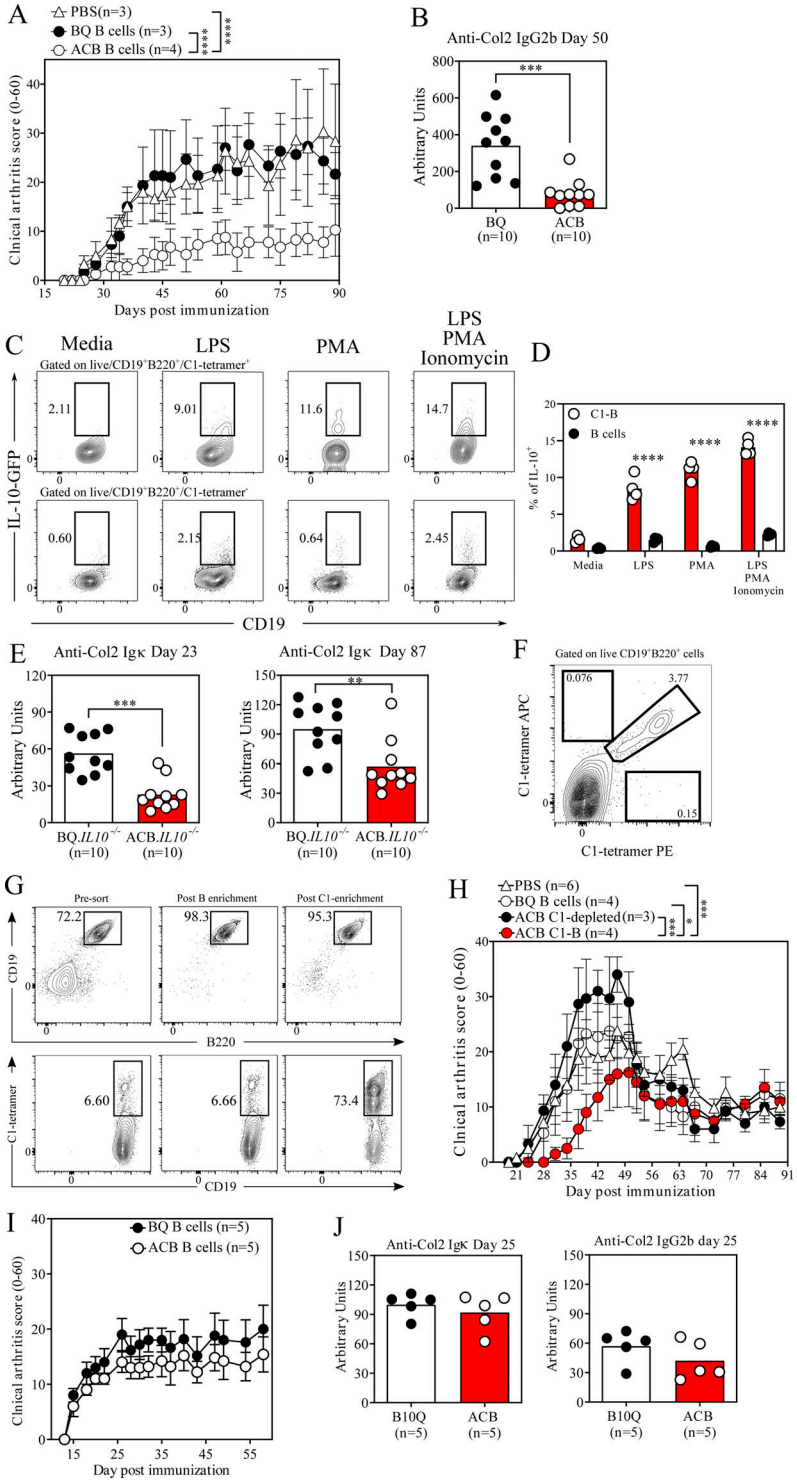

Figure S3. **Antibody response and IL10 production by C1-B. (A)** Adoptive transfer of naïve B cells from ACB and BQ mice into syngeneic autoimmune-prone BQ.*Ncf1*^{m1j} recipients. PBS group included where no adoptive transfer was carried out. Arthritis clinical score in recipient mice is plotted. **(B)** Titer of anti-COL2 antibody of IgG2b isotype measured by ELISA in the sera of recipient mice 50 d after CIA. **(C and D)** Comparative flow cytometric plots of C1^{+} and C1^{-} B cells depicting the frequency of IL10 production after in vitro stimulation using IL10-GFP reporter mice. **(E)** Titer of anti-COL2 IgG antibody measured by ELISA in the sera of recipient mice 23 and 87 d after CIA. **(F)** Frequency of C1-B in the spleen of ACB mice using dual tetramer staining. **(G)** Representative plot exhibiting the purity of magnetically enriched C1-B used for downstream procedures such as adoptive transfers. **(H)** Adoptive transfer of B cells from ACB (C1-B enriched or depleted) and BQ mice into syngeneic autoimmune-prone QD recipients. PBS group included where no adoptive transfer was carried out. Arthritis clinical score in recipient mice is plotted. **(I)** Adoptive transfer of B cells from ACB and BQ mice 10 d after CIA induction in syngeneic autoimmune-prone BQ.*Ncf1*^{m1j} mice. Arthritis clinical score in recipient mice is plotted. **(J)** Titer of anti-COL2 IgG antibody measured by ELISA in the sera of recipient mice 25 d after CIA. Error bars represent mean ± SEM. Statistical significance in A, B, E, and H–J was determined using two-tailed Mann–Whitney *U* test while in D was determined using one-way ANOVA followed by Sidak's correction test. *P < 0.05, **P < 0.01, ***P < 0.001, and ****P < 0.0001.

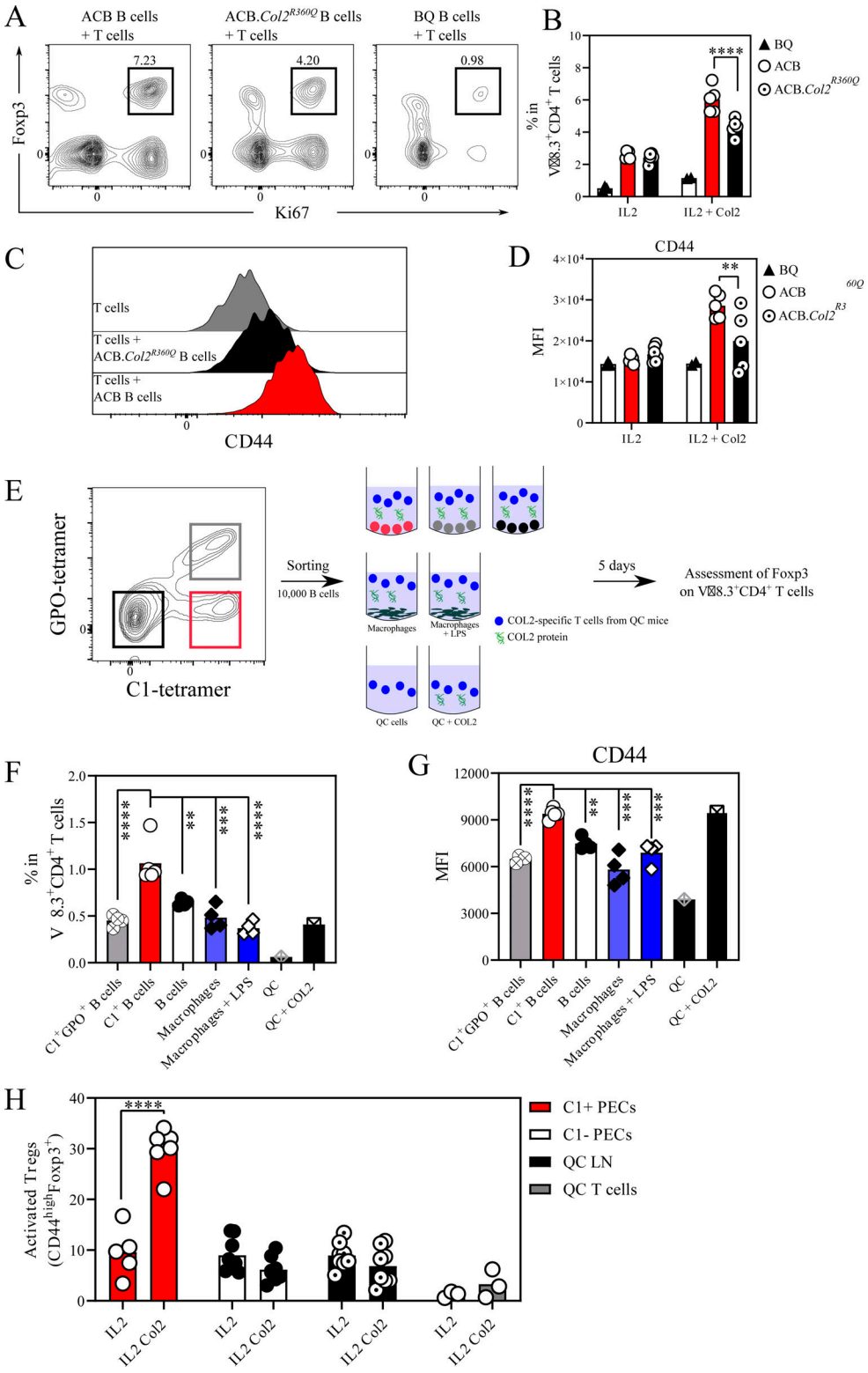

Figure S4. **C1-B controls the expansion of Tregs in vitro. (A)** Representative flow cytometry plot of the Foxp3⁺Ki67⁺ gating 48 h after coculture of sorted QC T cells with sorted B cells from ACB, ACB.*Col2*^{360Q}, or BQ WT mice in the presence or absence of COL2. **(B)** Frequency of proliferating Tregs within the Vβ8.3⁺CD4⁺ T cell population. **(C)** Representative histograms exhibiting the expression of CD44 on proliferating Tregs. **(D)** Quantification of CD44 MFI on proliferating Tregs from A. **(E)** Gating strategy and experimental design of the sorted 10,000 C1-B, C1-GPO-specific, and naïve B cells cocultured with sorted QC T cells for 5 d in the presence of COL2. **(F)** Frequency of Foxp3⁺ T cells within the Vβ8.3⁺CD4⁺ population. **(G)** Quantification of CD44 MFI on Tregs from F. **(H)** Frequency of activated Tregs within the Vβ8.3⁺CD4⁺ T cell population following coculture with C1-B (C1⁺), C1-B depleted (C1⁻), or without (total QC LN or isolated QC T cells alone) in the presence or absence of COL2. Error bars represent mean ± SEM. Statistical significance in B and D was determined using two-tailed Mann–Whitney *U* test while in F–H was determined using one-way ANOVA followed by Sidak's correction test. **P < 0.01 and ***P < 0.001.

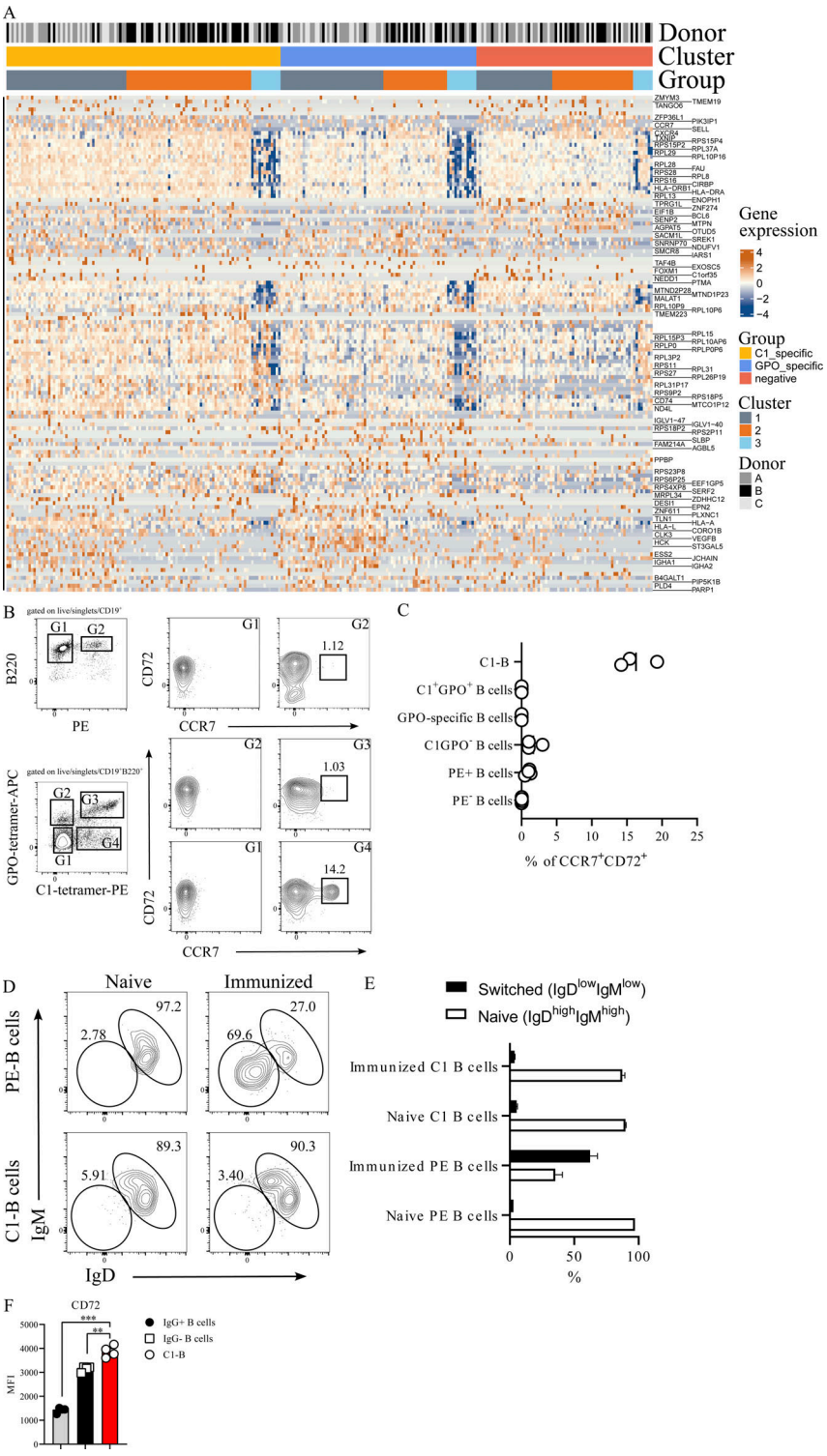

Figure S5. **CCR7/CD72 expression is restricted to autoreactive C1-B. (A)** Heatmap of the genes that are significantly expressed grouped according to the three donors (A, B, and C), the three B cell population groups (C1-specific, GPO-specific, and double negative B cells), and the three clusters (cluster 1 = memory cells, cluster 2 = naïve cells, cluster 3 = B1-like). Normalized log counts are plotted after scaling by row for the top 50 markers (Wilcoxon rank sum test, Scran). **(B)** Enriched PE-specific B cells and C1-B from spleens and iLN of BQ mice 10 d after immunization with PE and Col2, respectively. Naïve mice were also included. Representative flow cytometry plots exhibiting the surface expression of CD72 and CCR7 on different gated (G) populations. **(C)** Dot plot quantifying the frequency of CCR7/CD72 double-positive cells within the different gated populations. **(D)** Representative flow cytometry plots exhibiting IgM and IgD surface expression on PE- and C1- B cells enriched from naïve and 10 d immunized BQ mice. **(E)** Bar plot quantifying the frequency of naïve (IgD^{high}/IgM^{high}) and switched (IgD^{low}/IgM^{low}) C1- and PE-specific B cells enriched from naïve (n = 1–2/group) and 10 d immunized (n = 3/group) BQ mice. **(F)** MFI of surface CD72 on enriched C1-B, IgG^-, and IgG^+ B cells isolated from HD PBMC (n = 4). Error bars represent mean ± SEM. Statistical significance in F was determined using one-way ANOVA followed by Sidak's correction test. **P < 0.01, ***P < 0.001, and ****P < 0.0001.